Published for SISSA by Springer

Received: *June 24, 2010*
Revised: *September 3, 2010*
Accepted: *September 4, 2010*
Published: *October 13, 2010*

A geometric approach to CP violation: applications to the MCPMFV SUSY model

John Ellis,[a] **Jae Sik Lee**[b] **and Apostolos Pilaftsis**[c]

[a] *Theory Division, CERN, CH-1211 Geneva 23, Switzerland*
[b] *Physics Division, National Center for Theoretical Sciences, Hsinchu, 300 Taiwan*
[c] *School of Physics and Astronomy, University of Manchester, Manchester M13 9PL, United Kingdom*

E-mail: John.Ellis@cern.ch, jslee@phys.cts.nthu.edu.tw, apostolos.pilaftsis@manchester.ac.uk

Abstract: We analyze the constraints imposed by experimental upper limits on electric dipole moments (EDMs) within the Maximally CP- and Minimally Flavour-Violating (MCPMFV) version of the MSSM. Since the MCPMFV scenario has 6 non-standard CP-violating phases, in addition to the CP-odd QCD vacuum phase $\theta_{\rm QCD}$, cancellations may occur among the CP-violating contributions to the three measured EDMs, those of ^{205}Tl, the neutron and ^{199}Hg, leaving open the possibility of relatively large values of the other CP-violating observables. We develop a novel geometric method that uses the small-phase approximation as a starting point, takes the existing EDM constraints into account, and enables us to find maximal values of other CP-violating observables, such as the EDMs of the Deuteron and muon, the CP-violating asymmetry in $b \to s\gamma$ decay, and the B_s mixing phase. We apply this geometric method to provide upper limits on these observables within specific benchmark supersymmetric scenarios, including extensions that allow for a non-zero $\theta_{\rm QCD}$.

Keywords: Supersymmetry Phenomenology

ArXiv ePrint: 1006.3087

doi:10.1007/JHEP10(2010)049

JHEP10(2010)049

Contents

1 Introduction

The non-observation of electric dipole moments (EDMs) for Thallium (^{205}Tl) [1], the neutron (n) [2], and Mercury (^{199}Hg) [3, 4] provide very tight bounds on possible new sources of CP violation beyond the Cabibbo-Kobayashi-Maskawa (CKM) phase of the Standard Model (SM). *Prima facie*, these bounds suggest that any CP-violating phases associated with new physics at the TeV scale are very small, posing a challenge to scenarios of new TeV-scale physics, such as supersymmetry (SUSY) [5, 6], that contain many potential new sources of CP violation. The EDM challenge is compounded by the excellent agreement of present experiments with the CKM model [7], providing important complementary constraints on the flavour structure of any new TeV-scale physics, as well as on its role in CP violation. On the other hand, the baryon asymmetry in the Universe (BAU) could be explained by TeV-scale physics, if it has substantial CP violation and realizes a sufficiently strong first-order electroweak phase transition in the early Universe [8–11].

This tension between a TeV-scale origin of the BAU and EDMs will be explored both directly and indirectly in the LHC era. Experiments at the LHC, notably LHCb [12], will soon be giving direct new information about flavour and CP violation at the TeV scale. In parallel to these direct explorations at the LHC, a new generation of precision low-energy experiments will play an important indirect role. These new precision experiments will place much stronger indirect constraints on the possible CP and flavour structure of

JHEP10(2010)049

models of TeV-scale physics. New experiments on the neutron EDM are underway and, if the proposed experiment searching for a Deuteron ($^2H^+$) EDM achieves its design sensitivity [13, 14], it will improve the existing bounds on possible CP-violating chromoelectric operators by orders of magnitude [15].

In this paper we introduce a new geometric approach to the incorporation of EDM constraints on CP-violating models, showing how the maximal values of unmeasured CP-violating observables may be estimated in a systematic and reliable way. We illustrate this approach in the context of SUSY, regarding it as an archetype of the TeV-scale models that are (potentially) embarrassed by experimental constraints on flavour and CP violation. However, our geometric approach could easily be applied to other models, and indeed to other classes of observables besides those that violate CP.

For illustration, we work within the minimal supersymmetric extension of the Standard Model (MSSM), with SUSY broken softly at the TeV scale. We assume a generic version of this model with minimal flavour violation (MFV), driven by the fermion Yukawa couplings. As discussed in [16] and elaborated further in [17–23], this model has a total of 19 parameters, of which 6 violate CP. In the convention where both the superpotential Higgs-mixing parameter μ and the respective soft SUSY-breaking Higgs-mass term $B\mu$ are real, these are the three phases of the soft SUSY-breaking gaugino masses $M_{1,2,3}$ and the three phases of the trilinear SUSY-breaking parameters $A_{d,u,e}$. This model was called in [16] the Maximally CP- and Minimally Flavour-Violating (MCPMFV) scenario of the MSSM, or the MCPMFV SUSY model in short. In addition to the 6 MCPMFV phases, one may consider the CP-violating QCD vacuum phase $\theta_{\rm QCD}$. The specific question we study in this paper is how to find the maximum value of some other CP-violating observable, such as the CP-violating asymmetry in $b \to s\gamma$ decay, $A_{\rm CP}$, the phase in B_s mixing, ϕ_{B_s}, or some other EDM that has not yet been measured (accurately), such as those for the Deuteron and muon, while implementing the available EDM constraints.

In order to demonstrate the principle of our geometric approach, we first consider a toy warm-up problem involving a single constraint in a theory with three parameters. We characterize the subspace of parameters satisfying this constraint in the linear approximation, and then show how to identify the direction in this subspace that maximizes any given observable O. The generalization to multiple constraints in higher-dimensional spaces follows similar geometric principles, that may be described in the language of exterior products of differential forms [24]. This geometric optimization method of the so-called "cancellation mechanism" [25, 26] may sound complicated, but its numerical implementation is straightforward. We emphasize that our geometric approach differs in principle from the naive scan method that is usually adopted in the literature [18, 27–32]. The geometric method proposed here provides an accurate parametric determination of the optimal cancellation regions where any given physical observable is maximized in the linear approximation. Hence, our geometric approach is exact, efficient and less computationally-intensive than a naive scan of a multi-dimensional space.

In the application of this approach to the MCPMFV SUSY model, we first select some benchmark points in the CP-conserving restriction of the model. We then evaluate the dependences of the relevant constraints (the EDMs of ^{205}Tl, the neutron and ^{199}Hg) on the

JHEP10(2010)049

six CP-violating phases of the full MCPMFV model in the linear approximation, as well as the linear dependences of the CP-violating observables of interest (the Deuteron and muon EDMs, $A_{\rm CP}$ and ϕ_{B_s}). We then demonstrate numerically how each of these observables may be maximized in the linear approximation, taking into account the existing EDM constraints. We note that, at any specific benchmark point, the values of all CP-violating observables are bounded in magnitude, since the ranges of the CP-violating phases ϕ_i are all compact: $\phi_i \in [0, 2\pi)$. We also note that our approach is only approximate for large CP-violating phases. Nevertheless, the linear expansions give good estimates of the true maximal values of the CP-violating observables.

We find that the linear approximations to the EDMs and other CP-violating observables in the neighbourhoods of the MCPMFV benchmark points we study are quite accurate for CP-violating angles with magnitudes up to several tens of degrees. We confirm that the EDM-free directions in parameter space constructed using our geometric construction yield values of the other CP-violating observables that are larger than those possible (in the linear approximation) along other directions in the space of CP-violating phases. Along the optimal EDM-free directions, we find that values of the Deuteron EDM an order of magnitude larger than the prospective experimental sensitivity may be attained for acceptable values of the MCPMFV phases, and almost an order of magnitude larger still if the optimal geometric construction is extended to include the CP-violating QCD vacuum phase $\theta_{\rm QCD}$. On the other hand, we find maximal values of the muon EDM that are below the likely experimental sensitivity in both the scenarios with and without the QCD phase. In the case of $A_{\rm CP}$, we find values as large as 2% in the large $\tan\beta$ scenario. Given the constraint from $B(b \to s\gamma)$, however, $A_{\rm CP}$ cannot exceed the 0.1% level and so remains too small to be observed. Finally, the B_s-meson mixing phase ϕ_{B_s} turns out to be close to the small SM value in both the scenarios studied.

The layout of the paper is as follows. Section 2 presents our novel geometric approach, starting with the toy three-dimensional exercise and continuing to the six-dimensional case of the MCPMFV SUSY model. The implementation of this approach for a selection of benchmark points is described in section 3, and our numerical results for $A_{\rm CP}$, ϕ_{B_s} and the Deuteron and muon EDMs are presented in section 4. Section 5 extends the previous discussion to the seven-dimensional case including $\theta_{\rm QCD}$. Finally, section 6 presents our conclusions and some suggestions for future work.

2 Optimal EDM-free directions

The current experimental upper bounds on the Thallium, neutron and Mercury EDMs put very strict constraints on the CP-violating parameters of the theory, such as CP-odd phases. However, they do not constrain all possible combinations of the CP-violating phases in models with many such phases, such as the MSSM. It is therefore important to develop a powerful approach for finding the optimal choice of CP-odd phases which maximize the size of a given CP-violating observable O, while remaining compatible with the present EDM constraints. Examples of such CP-violating observables for which the

JHEP10(2010)049

present experimental sensitivities are likely soon to be improved significantly include the Deuteron and muon EDMs, the CP asymmetry in $b \to s\gamma$, and the phase in B_s mixing.

In this paper, we propose a geometric approach to the maximization of such observables, which may also be applied to other analogous problems. For illustration, we first consider a simple three-dimensional (3D) example for a theory which has only three physical CP-odd phases. Working in the 3D vector space defined by these three CP-odd phases, we show how to construct geometrically optimal 'EDM-free' directions in the small-phase approximation. We then generalize this approach to theories with more than three CP-odd phases, such as the MCPMFV SUSY model with its six new CP-odd phases, optionally including the QCD vacuum phase $\theta_{\rm QCD}$. Using simple ideas from the calculus of differential forms [24] for such a higher-dimensional setup, we are able to derive the optimal EDM-free directions for any given CP-violating observable O that we wish to study.

2.1 A simple 3D example

For the sake of geometric familiarity, we first consider the simple 3D example of a theory with just three physical CP-odd phases, represented by the 3D phase vector $\mathbf{\Phi} = (\Phi_1, \Phi_2, \Phi_3)$. For illustration, we assume that we have a single very stringent EDM constraint, which we denote by E. In the region of small phases, e.g., for $|\mathbf{\Phi}| \lesssim \pi/6$, we seek to maximize the value of some specific CP-violating observable O, under the condition $E = 0$. Both the CP-violating observable O and the EDM constraint E are functions of $\mathbf{\Phi}$, i.e., $O = O(\mathbf{\Phi})$ and $E = E(\mathbf{\Phi})$, and vanish in the limit of vanishing CP-odd phases: $O(\mathbf{0}) = 0$, $E(\mathbf{0}) = 0$.[1]

We make Taylor expansions of O and E in terms of the small phases, and keep only the linear terms in these expansions:

$$O \;=\; \mathbf{\Phi} \cdot \mathbf{O}\,, \qquad E \;=\; \mathbf{\Phi} \cdot \mathbf{E}\,, \tag{2.1}$$

where we have defined $\mathbf{O} \equiv \nabla O$, $\mathbf{E} \equiv \nabla E$, and $\nabla \equiv (\partial/\partial\phi_1, \partial/\partial\phi_2, \partial/\partial\phi_3)$. The condition $E = 0$ requires that the phase vector $\mathbf{\Phi}$ should lie in the plane orthogonal to $\mathbf{E}$. In order to maximize the value of O, the phase vector $\mathbf{\Phi}$ should lie along the intersection of the plane spanned by the vectors $\mathbf{O}$ and $\mathbf{E}$ with this plane perpendicular to $\mathbf{E}$, as represented schematically in figure 1. Up to an overall sign, the solution is unique and is given by the double cross-product:

$$\mathbf{\Phi^*} \;=\; \mathbf{E} \times \Big(\mathbf{O} \times \mathbf{E} \Big)\,. \tag{2.2}$$

Evidently, the condition $E = 0$ is satisfied by construction in the small-phase approximation, i.e., $E \equiv \mathbf{\Phi^*} \cdot \mathbf{E} = 0$. In this way, we can construct unambiguously the optimal EDM-free direction $\mathbf{\Phi^*}$.

It is straightforward to obtain the maximum value of the CP-violating observable O. In the small-phase approximation, this is simply given by

$$O \;=\; \phi^* \, \widehat{\mathbf{\Phi}}^* \cdot \mathbf{O} \;=\; \pm\, \phi^* \, \sqrt{|\mathbf{O}|^2 \;-\; (\mathbf{O} \cdot \widehat{\mathbf{E}})^2}\,, \tag{2.3}$$

[1] Our approach can easily be extended to cases where some of the phases $\Phi_{1,2,3}$ approach another CP-conserving point different from zero, e.g., $\Phi_{1,2,3} \to \pm\pi$, in which case the CP-odd phase vector $\mathbf{\Phi}$ represents the difference from this CP-conserving point.

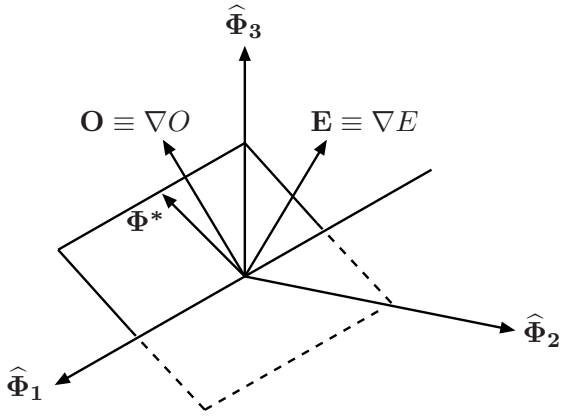

Figure 1. Geometric construction of the optimal EDM-free direction in the small-phase approximation for a CP-violating observable O, subject to the EDM constraint $E = 0$, in a theory with three physical CP-odd phases $\Phi_{1,2,3}$. The optimal EDM-free direction is given by the CP-odd phase vector $\mathbf{\Phi^*}$, which is the intersection of the indicated plane perpendicular to the vector $\mathbf{E}$ with the plane defined by the vectors $\mathbf{O}$ and $\mathbf{E}$.

where $\phi^* \equiv |\mathbf{\Phi^*}|$ and the carets on the vectors indicate unit-norm vectors. In the small-phase approximation, the largest possible value for the CP-violating observable O is obtained when $\mathbf{E}$ is perpendicular to $\mathbf{O}$, in which case we have

$$O_{\rm max} \;=\; \pm\, \phi^*\, |\mathbf{O}|\;. \tag{2.4}$$

On the other extreme, if $\mathbf{E}$ happens to be parallel to $\mathbf{O}$, then the CP-violating observable O vanishes, i.e., $O = 0$, in the limit that $E = 0$. Note that there is a twofold degeneracy in the optimal value of the CP-violating observable O, i.e., our geometric construction leaves O undetermined up to an overall sign. However, this twofold degeneracy is a consequence of the linear small-phase approximation, where quadratic and higher-order derivative terms in a Taylor series expansion, e.g., $\nabla_i \nabla_j E$, were neglected. These terms break this twofold degeneracy in general, and we include them all in our numerical analysis.

2.2 A 6D example: the MCPMFV SUSY model

The above geometric construction for the 3D example can be generalized to theories with more than three CP-odd phases, such as the MCPMFV SUSY model, which has six phases,[2] and including more than one EDM constraint. In the case of such a theory with six CP-odd phases, $\mathbf{\Phi}$ is now a 6D phase vector, subject to three EDM constraints denoted by $E^{a,b,c} = 0$, corresponding to the non-observation of the Thallium, neutron and Mercury EDMs. As before, the task is to maximize a given CP-violating observable O, now satisfying simultaneously the three conditions: $E^a = E^b = E^c = 0$.

The generalization of the differential operator ∇ to 6 dimensions is obvious, and it may be used to obtain in the small-phase approximation the four 6D vectors: $\mathbf{E}^{a,b,c} =$

[2]We extend this discussion later to include the QCD phase $\theta_{\rm QCD}$.

JHEP10(2010)049

$\nabla E^{a,b,c}$ and $\mathbf{O} = \nabla O$. For simplicity, we assume that the four vectors $\mathbf{E}^{a,b,c}$ and $\mathbf{O}$ are linearly independent, i.e., there are no degeneracies between the EDM constraints and the observable O: we return to this issue towards the end of this section.

Given the above assumptions, the analogue of the single vector $\mathbf{E}$ in the 3D example is the triple exterior product

$$A_{\alpha\beta\gamma} \;=\; E^a_{[\alpha}\, E^b_\beta\, E^c_{\gamma]}\;, \tag{2.5}$$

where the Greek indices label the components of the vectors in the 6D space, i.e., $\alpha,\ \beta,\ \gamma = 1, 2, \ldots, 6$. The square brackets on the r.h.s. of (2.5) indicate that the tensor $A_{\alpha\beta\gamma}$ is obtained by fully antisymmetrizing the vectors E^a_α, E^b_β and E^c_γ in the indices α, β, γ, i.e., $A_{\alpha\beta\gamma} = -A_{\beta\alpha\gamma} = -A_{\alpha\gamma\beta}$ etc. Borrowing a term from the calculus of differential forms, $A_{\alpha\beta\gamma}$ is a 3-form.

Correspondingly, the analogue of the direction $\mathbf{O} \times \mathbf{E}$, which determines the normal to the plane defined by $\mathbf{O}$ and $\mathbf{E}$ in the 3D example described above, is the 2-form

$$B_{\mu\nu} \;=\; \varepsilon_{\mu\nu\lambda\rho\sigma\tau}\, O_\lambda\, E^a_\rho\, E^b_\sigma\, E^c_\tau\;, \tag{2.6}$$

where summation over repeated indices is implied and $\varepsilon_{\mu\nu\lambda\rho\sigma\tau}$ is the usual Levi-Civita tensor generalized to 6D. In the language of differential forms, $B_{\mu\nu}$ is, up to an irrelevant overall factor, the Hodge-dual product between the 1-form O_λ, representing the CP-violating observable, and the 3-form $A_{\alpha\beta\gamma}$.

The components Φ^*_α of the optimal EDM-free direction maximizing O can now be obtained from the Hodge-dual product of the 3-form $A_{\beta\gamma\delta}$ and the 2-form $B_{\mu\nu}$. Explicitly,

$$\Phi^*_\alpha \;=\; \mathcal{N}\, \varepsilon_{\alpha\beta\gamma\delta\mu\nu}\, A_{\beta\gamma\delta}\, B_{\mu\nu} \;=\; \mathcal{N}\, \varepsilon_{\alpha\beta\gamma\delta\mu\nu}\, \varepsilon_{\mu\nu\lambda\rho\sigma\tau}\, E^a_\beta\, E^b_\gamma\, E^c_\delta\, O_\lambda\, E^a_\rho\, E^b_\sigma\, E^c_\tau\,, \tag{2.7}$$

where we have included an unknown overall normalization factor $\mathcal{N}$. By construction, the 6D phase vector $\mathbf{\Phi^*}$ is orthogonal to the three vectors $\mathbf{E}^{a,b,c}$, thus satisfying the desired EDM constraints, $E^a = E^b = E^c = 0$, in the small-phase approximation. We observe that the magnitude $\phi^* \equiv |\mathbf{\Phi^*}|$, and hence the overall normalization factor $\mathcal{N}$, can only be determined by a numerical analysis of the actual experimental limits on the three EDMs. As in the 3D example, the maximum allowed value of the CP-violating observable O is given in the small-phase approximation by

$$O \;=\; \phi^*\, \widehat{\Phi}^*_\kappa\, O_\kappa \;=\; \pm\, \mathcal{N} \left| \varepsilon_{\mu\nu\alpha\beta\gamma\delta}\, \varepsilon_{\mu\nu\lambda\rho\sigma\tau}\, O_\alpha\, O_\lambda\, E^a_\beta\, E^b_\gamma\, E^c_\delta\, E^a_\rho\, E^b_\sigma\, E^c_\tau \right|\,, \tag{2.8}$$

where the caret denotes the components of a unit-norm vector. As in the 3D case, quadratic and higher-order derivative terms with respect to the CP-odd phases will generically prefer a particular sign for the optimal value of O.[3]

As a consistency check of our geometric construction, one may verify that in the small-angle approximation the largest possible value, $O_{\max} = \pm\, \phi^* |\mathbf{O}|$, is obtained when all the four 6D vectors, $\mathbf{O}$ and $\mathbf{E}^{a,b,c}$, are mutually orthogonal, exactly as in the 3D case. For example, if the vectors $\mathbf{E}^{a,b,c}$ have non-zero components only in the 4, 5 and 6 directions,

[3] In some circumstances, the small-phase approximation may even break down in such a way that the maximal value of O is obtained for a value of ϕ^* less than the maximal value allowed by E.

JHEP10(2010)049

respectively, and the CP-violating observable O is a reduced 3-vector living in the 1, 2 and 3 coordinates, it is not difficult to check that the expression (2.8) gives the largest possible value $O_{\rm max}$, as expected.

The above geometric construction can be extended to include further EDM or other strict CP-violating constraints on the theory. Specifically, in the MCPMFV SUSY model, we can afford to have at least two more linearly-independent constraints coming from different experiments and still be able to potentially get one large combination of CP-odd phases. If $E^{d,e} = 0$ are these two extra constraints, the maximum allowed value for the CP-violating observable O will then be

$$O \;=\; \pm\,\mathcal{N}\left|\varepsilon_{\mu\nu\alpha\beta\gamma\delta}\; O_\mu\, E^a_\nu\, E^b_\alpha\, E^c_\beta\, E^d_\gamma\, E^e_\delta\right|\,, \tag{2.9}$$

where the normalization $\mathcal{N}$ depends on the actual size of ϕ^*. Equation (2.9) is nothing else than the simple generalization of the well-known triple-product to 6D.

We can also allow for the possible presence of a non-zero strong CP phase $\theta_{\rm QCD}$ in the theory, in which case the corresponding CP-odd phase vector $\mathbf{\Phi}$ becomes seven-dimensional (7D) in the MCPMFV SUSY model. In this case, four additional linearly-independent EDMs or other strict CP-violating constraints would be needed, in addition to the three limits from the present EDM experiments, in order to span fully the CP-odd space of the MCPMFV model, and so constrain the norm of the 7D CP-odd phase vector $\mathbf{\Phi}$ as discussed in section 5.

In our geometric construction, an important role is played by the degree of degeneracy, or alignment, between pairs of observables, e.g., between O and the E^a. For this purpose, it is interesting to know the cosine $C_{\mathbf{O},\mathbf{E}^a}$ of the relative angle between their corresponding vectors $\mathbf{O}$ and $\mathbf{E}^a$, i.e.,

$$C_{\mathbf{O},\mathbf{E}^a} \;=\; \frac{\mathbf{O}\cdot\mathbf{E}^a}{|\mathbf{O}|\,|\mathbf{E}^a|}\;. \tag{2.10}$$

If $C_{\mathbf{O},\mathbf{E}^a} = \pm 1$, we have perfect alignment of the observables O and E^a. In such a case, if E^a vanishes, then so does O. On the other hand, if $C_{\mathbf{O},\mathbf{E}^a} = 0$, the two observables O and E^a are orthogonal, and hence can vary independently of each other. Using (2.10), one can obtain an upper bound for the optimal value of the CP-violating observable O in the small-phase approximation:

$$|O| \;\leq\; \phi^*\left[1 \;-\; \mathrm{Max}\left(C^2_{\mathbf{O},\mathbf{E}^x}\right)\right]^{1/2}\,|\mathbf{O}|\,, \tag{2.11}$$

where the index x labels the vectors $\mathbf{E}^{a,b,c,\cdots}$ related to the different EDM constraints. Notice that the inequality (2.11) becomes an exact equality in the 3D example which we discussed before in section 2.1 [cf. (2.3)].

Finally, after completing the description of this geometric approach, we note that it could be applied to many other phenomenological problems where there are M constraints on a theory with $N > M$ parameters, and one wishes to determine the maximum value of some other observable quantity.

JHEP10(2010)049

3 Numerical illustrations

In this section we illustrate the geometric approach introduced in section 2 by constructing optimal EDM-free directions for some specific benchmark scenarios. For this purpose, we consider CP-violating variants of a typical CMSSM scenario with

$$\begin{aligned} |M_{1,2,3}| &= 250 \ \ \text{GeV}\,, \\ M_{H_u}^2 &= M_{H_d}^2 = \widetilde{M}_Q^2 = \widetilde{M}_U^2 = \widetilde{M}_D^2 = \widetilde{M}_L^2 = \widetilde{M}_E^2 = (100 \ \ \text{GeV})^2\,, \\ |A_u| &= |A_d| = |A_e| = 100 \ \ \text{GeV}\,, \end{aligned} \tag{3.1}$$

at the GUT scale, introducing non-zero CP-violating phases and varying $\tan\beta\,(M_{\rm SUSY})$. We adopt the convention that $\Phi_\mu = 0°$, and we vary independently the following six MCPMFV phases at the GUT scale: Φ_1, Φ_2, Φ_3, Φ_{A_u}, Φ_{A_d}, and Φ_{A_e}. We note that the $\Phi_{1,2,3}$, and the μ parameter, Φ_μ, are unchanged by the RG evolution at the one-loop level, whereas the phases of the trilinear couplings $\mathbf{A}_{u,d,e}$ at low scales could be significantly different from the values specified at the GUT scale. This scenario becomes the SPS1a point [33–36] when $\tan\beta = 10$, $\Phi_{1,2,3} = 0°$ and $\Phi_{A_u,A_d,A_e} = 180°$. Our calculations of the EDMs include the two-loop diagrams mediated by the γ-$H^\pm$-$W^\mp$ and γ-$W^\pm$-$W^\mp$ couplings, which are summarized in the appendix. Unlike [37, 38], we incorporate the Φ_3 dependence induced by gluino exchange in the one-loop $H^\pm$-u-d coupling, which becomes relevant in the region of large $\tan\beta$.

In order to analyze this scenario, we first make Taylor expansions of the following five EDMs and two CP-violating observables:

$$\begin{aligned} &d_{\rm Tl}/d_{\rm Tl}^{\rm EXP}\,, \quad d_{\rm n}/d_{\rm n}^{\rm EXP}\,, \quad d_{\rm Hg}/d_{\rm Hg}^{\rm EXP}\,, \quad d_{\rm D}/d_{\rm D}^{\rm EXP}\,, \quad d_\mu/d_\mu^{\rm EXP}\,, \\ &A_{\rm CP}(b\to s\gamma)[\%]\,, \quad \phi_{B_s} \equiv \text{Arg}\left(\langle \bar{B}_s^0|\mathcal{H}_{\rm eff}^{\Delta B=2}|B_s^0\rangle_{\rm SUSY}\right)[°]\,, \end{aligned} \tag{3.2}$$

where we choose the following normalization factors

$$\begin{aligned} &d_{\rm Tl}^{\rm EXP} = 9\times10^{-25}\,e\,\text{cm}\,, \quad d_{\rm n}^{\rm EXP} = 3\times10^{-26}\,e\,\text{cm}\,, \quad d_{\rm Hg}^{\rm EXP} = 3.1\times10^{-29}\,e\,\text{cm}\,, \\ &d_{\rm D}^{\rm EXP} = 3\times10^{-27}\,e\,\text{cm}\,, \quad d_\mu^{\rm EXP} = 1\times10^{-24}\,e\,\text{cm}. \end{aligned} \tag{3.3}$$

In the cases of the EDMs of Thallium [1], the neutron [2], and Mercury [3, 4], we use the current experimental limits for normalization, and for the EDMs of Deuteron and muon we use the sensitivities projected in [13, 39]. The observables $A_{\rm CP}$ and ϕ_{B_s} are measured in percent and degrees, respectively.

In order to obtain the vectors representing the EDM constraints and the observables in the six-dimensional CP-phase space, namely $\mathbf{E} = \nabla E$ and $\mathbf{O} = \nabla O$ where

$$\nabla_\alpha \equiv (\partial/\partial\Phi_1, \partial/\partial\Phi_2, \partial/\partial\Phi_3, \partial/\partial\Phi_{A_u}, \partial/\partial\Phi_{A_d}, \partial/\partial\Phi_{A_e})\,, \tag{3.4}$$

we calculate the EDMs and the observables in ranges $\Delta\Phi = \pm10°$ around each chosen CP-conserving point $\widetilde{\varphi}_\alpha$, varying independently each of the six CP phases, and performing a quadratic fit in each case. As an example, figure 2 shows a quadratic fit to the Thallium EDM for the scenario under consideration taking $\tan\beta = 40$. We observe that the

JHEP10(2010)049

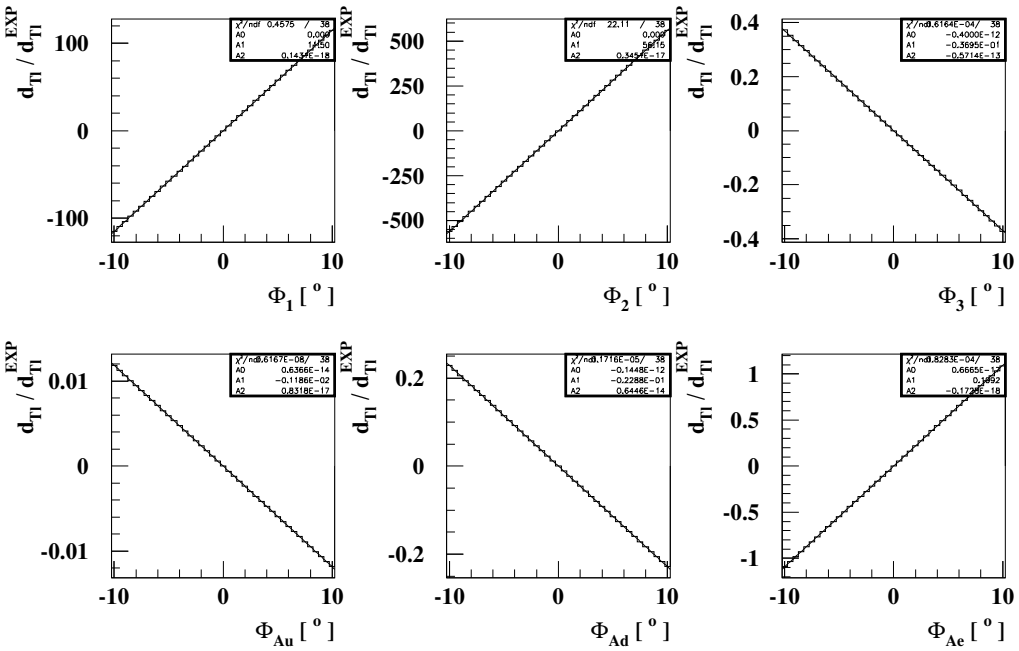

Figure 2. The quadratic fit to the Thallium EDM that is used to obtain the 6D vector $\mathbf{E}^{d_{\rm Tl}} \equiv \nabla(d_{\rm Tl}/d_{\rm Tl}^{\rm EXP})$ in an expansion around $\widetilde{\varphi}_\alpha = 0°$ for the scenario (3.1) with $\tan\beta = 40$.

CP-violating phase dependence is in fact linear in the region considered, to a very good approximation.

In figures 3 and 4, we show the absolute values of the components of the six 6D vectors

$$\begin{aligned} &\mathbf{E}^{d_{\rm Tl}} \equiv \nabla(d_{\rm Tl}/d_{\rm Tl}^{\rm EXP})\,, \quad \mathbf{E}^{d_{\rm n}} \equiv \nabla(d_{\rm n}/d_{\rm n}^{\rm EXP})\,, \quad \mathbf{E}^{d_{\rm Hg}} \equiv \nabla(d_{\rm Hg}/d_{\rm Hg}^{\rm EXP})\,; \\ &\mathbf{O}^{d_{\rm D}} \equiv \nabla(d_{\rm D}/d_{\rm D}^{\rm EXP})\,, \quad \mathbf{O}^{d_\mu} \equiv \nabla(d_\mu/d_\mu^{\rm EXP})\,, \quad \mathbf{O}^{A_{\rm CP}} \equiv \nabla(A_{\rm CP}/\%)\,, \end{aligned} \tag{3.5}$$

around the CP-conserving points $\widetilde{\varphi}_\alpha = 0°$ and $\widetilde{\varphi}_\alpha = 180°$, respectively, varying $\tan\beta$. We do not show $\mathbf{O}^{\phi_{B_s}}$, since we find that this observable is too small to be detectable in the class of scenarios under consideration. The solid lines are for the components of the CP-violating phases of the gaugino mass parameters ($\alpha = 1,2,3$) and the dashed lines for those of the trilinear A parameters ($\alpha = 4,5,6$). The dominant components are $\left(\mathbf{E}^{d_{\rm Tl}}\right)_{2,1}$, $\left(\mathbf{E}^{d_{\rm n}}\right)_{2,3}$, $\left(\mathbf{E}^{d_{\rm Hg}}\right)_{3,2}$, $\left(\mathbf{O}^{d_{\rm D}}\right)_{3,2}$, $\left(\mathbf{O}^{d_\mu}\right)_{2,1}$, and $\left(\mathbf{O}^{A_{\rm CP}}\right)_{3,2}$, reflecting strong dependences on the CP-violating phases of the gaugino mass parameters. The $\Phi_{1,2,3}$ components grow as $\tan\beta$ increases, implying that the EDM constraints on the CP phases $\Phi_{1,2,3}$ become stronger for larger $\tan\beta$. On the other hand, the Φ_{A_u,A_d,A_e} components are less than unity, except for $\mathbf{O}^{d_{\rm D}}$. This implies that the EDM constraints on these phases are weaker, and that the Deuteron EDM may be large enough to be observed in the proposed experiment. We also observe that the component $\left(\mathbf{O}^{A_{\rm CP}}\right)_{A_u} > 10^{-2}$ when $\tan\beta \gtrsim 30$ and $\widetilde{\varphi}_\alpha = 0°$, implying that it could give rise to the CP asymmetry larger than 1 % when $\Phi_{2,3} \sim 0°$ but Φ_{A_u} is large, about 100°.

In figure 5, we display the cosines $C_{\mathbf{O},\mathbf{E}^a}$ of the relative angles between the three observable vectors $\mathbf{O}^{d_{\rm D},d_\mu,A_{\rm CP}}$ and the three EDM-constraint vectors $\mathbf{E}^{d_{\rm Tl},d_{\rm n},d_{\rm Hg}}$. The

JHEP10(2010)049

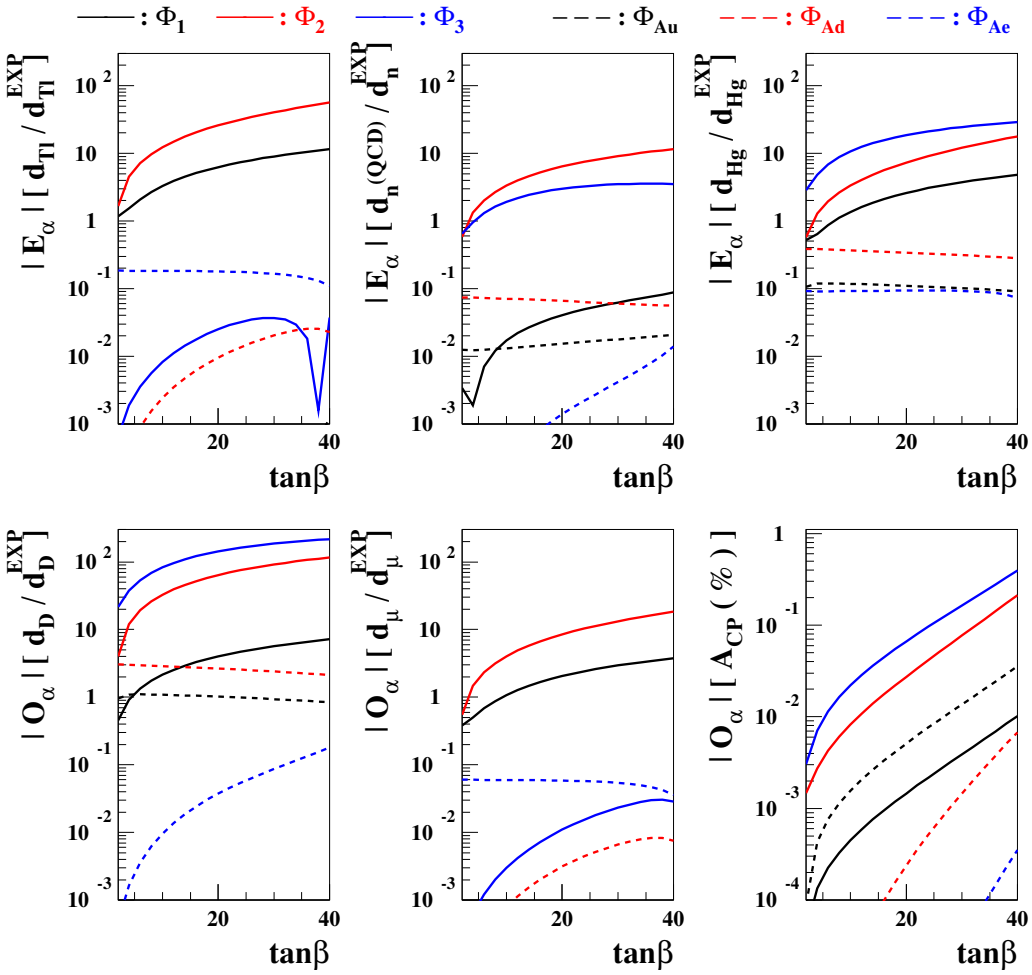

Figure 3. The absolute values of the components of the three 6D vectors representing the present EDM constraints (upper), and those of the three 6D vectors representing other CP-violating observables (lower) in expansions around the CP-conserving point $\widetilde{\varphi}_\alpha = 0°$ as functions of $\tan\beta$ for the scenario (3.1). The black, red, and blue solid lines are for the components of Φ_1, Φ_2, and Φ_3, respectively, and the black, red, and blue dashed lines for the components of Φ_{A_u}, Φ_{A_d}, and Φ_{A_e}, respectively.

upper frames are for the case of $\widetilde{\varphi}_\alpha = 0°$ and the lower ones for $\widetilde{\varphi}_\alpha = 180°$. We see that the cosines between the observables and $\mathbf{E}^{d_{\rm Tl}}$ (black solid lines) are reasonably small, except the case of the muon EDM. In the case, the Thallium EDM is dominated by the electron EDM, resulting in the high degeneracy between the Thallium EDM constraint and the muon EDM.[4] This alignment between the Thallium and muon EDMs in the scenario under consideration leads to a prediction of the muon EDM that is below the projected sensitivity, as we show in the next section. On the other hand, the cosines between the $\mathbf{O}^{d_{\rm D}, A_{\rm CP}}$ and

[4]The two EDMs are not exactly degenerate, due to the additional contribution to $d_{\rm Tl}$ from the electron-Nucleon interaction $C_S\,\bar{e}i\gamma_5\,e\,\bar{N}N$, which becomes larger as $\tan\beta$ increases. We find that the degeneracy is lifted by an amount of $\mathcal{O}(10^{-4})$ for large $\tan\beta$, which it is too small to have visible effect in the figure.

JHEP10(2010)049

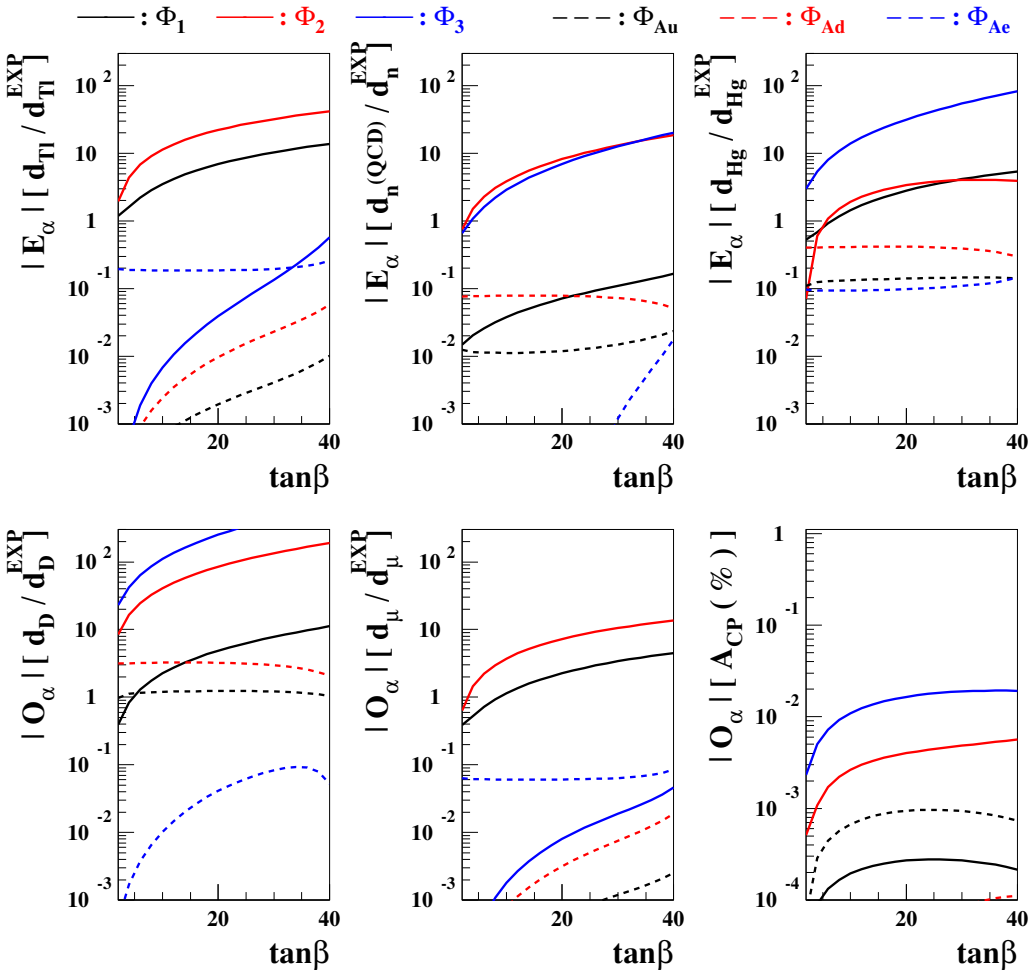

Figure 4. The same as in figure 3 but for expansions around the CP-conserving point $\widetilde{\varphi}_\alpha = 180°$.

$\mathbf{E}^{d_n}$ (red dashed lines) are larger than those between $\mathbf{O}^{d_D, A_{CP}}$ and $\mathbf{E}^{d_{Hg}}$ (blue dash-dotted lines) for $\widetilde{\varphi}_\alpha = 0°$. In the case $\widetilde{\varphi}_\alpha = 180°$, the cosines between the observable and the Mercury EDM-constraint vectors are slightly larger.

Having the vectors representing the EDM constraints and observables in hand, one can combine them to construct the optimal directions in the 6D space of CP-violating phases, using eq. (2.7). Specifically, we consider the three optimal directions that maximize d_D, d_μ, and A_{CP}, respectively, taking into account the three existing EDM constraints. As comparisons to them, we also consider two other reference directions, which have $\Delta\Phi_1 = \Delta\Phi_{A_e} = 0$ and $\Delta\Phi_2 = \Delta\Phi_3 = 0$, where $\Delta\Phi$ denotes the difference from the corresponding CP-conserving point. These two reference directions can be constructed by defining

$$\Phi^*_\alpha \equiv \mathcal{N}\, \varepsilon_{\alpha\beta\gamma\delta\mu\nu}\, E^a_\beta\, E^b_\gamma\, E^c_\delta\, N^{(1)}_\mu\, N^{(2)}_\nu\,, \tag{3.6}$$

JHEP10(2010)049

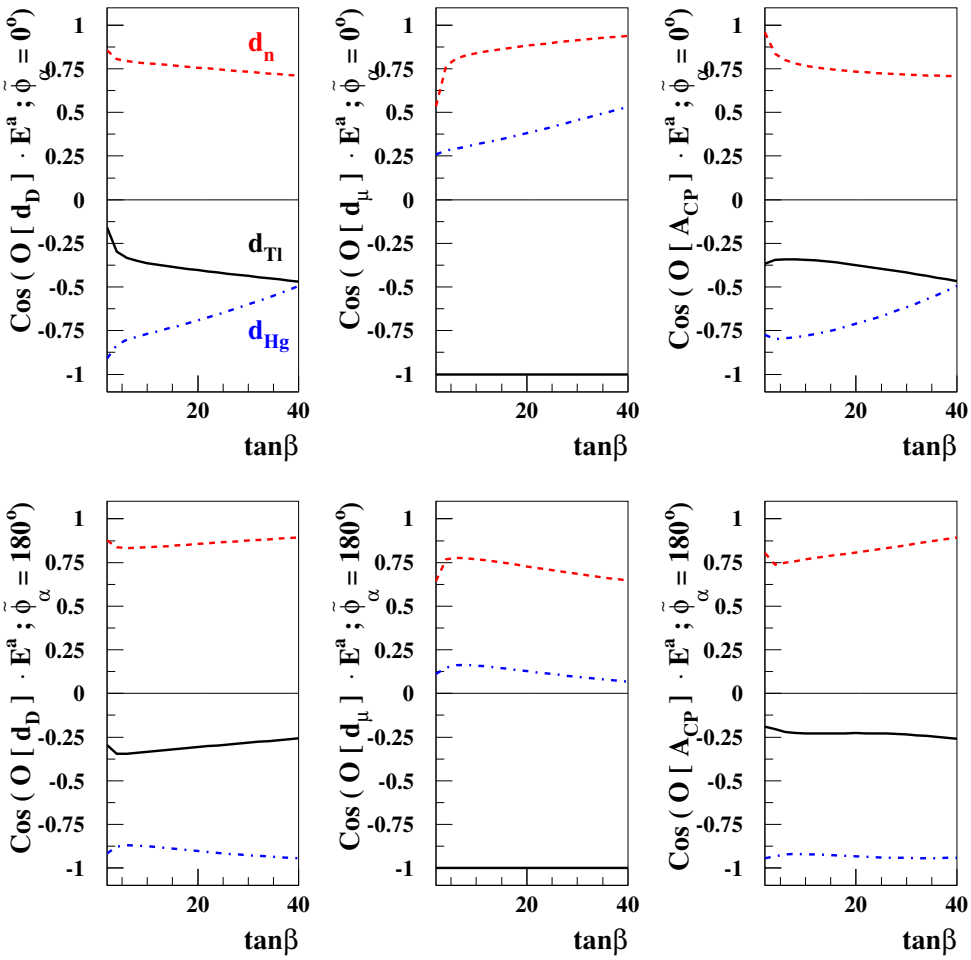

Figure 5. The cosines between the three observable vectors $\mathbf{O}^{d_{\rm D},d_\mu,A_{\rm CP}}$ (left, middle, right frames) and the three EDM-constraint vectors $\mathbf{E}^{d_{\rm Tl},d_{\rm n},d_{\rm Hg}}$ (solid, dashed, dash-dotted lines) as functions of $\tan\beta$ for $\widetilde{\varphi}_\alpha = 0°$ (upper) and $\widetilde{\varphi}_\alpha = 180°$ (lower).

where, for each direction, the two null directions $N_\mu^{(1,2)}$ are chosen as

$$\begin{aligned} &N_\mu^{(1)} = (1,0,0,0,0,0)\,, N_\mu^{(2)} = (0,0,0,0,0,1) \;\text{ for the direction } \Delta\Phi_1 = \Delta\Phi_{A_e} = 0, \\ &N_\mu^{(1)} = (0,1,0,0,0,0)\,, N_\mu^{(2)} = (0,0,1,0,0,0) \;\text{ for the direction } \Delta\Phi_2 = \Delta\Phi_3 = 0\ . \end{aligned} \tag{3.7}$$

We show in figures 6 and 7 the absolute values of the six components of the five normalized vectors for $\widetilde{\varphi}_\alpha = 0°$ and $\widetilde{\varphi}_\alpha = 180°$, respectively. We first observe that the $\Phi_{1,2,3}$ components (solid lines) are relatively small, and decrease as $\tan\beta$ increases. Hence, all the directions are mostly given by some combination of Φ_{A_u} (black dashed line) and Φ_{A_d} (red dashed line) directions, with the exception of the $\Delta\Phi_{2,3} = 0$ direction, which is mainly aligned with the Φ_{A_e} (blue dashed line) direction. The Φ_{A_u} component is generally larger than the Φ_{A_d} component in the optimal directions, except in the case of d_μ with $\widetilde{\varphi}_\alpha = 0°$ and $\tan\beta \gtrsim 20$, as seen in the middle-upper frame of figure 6.

JHEP10(2010)049

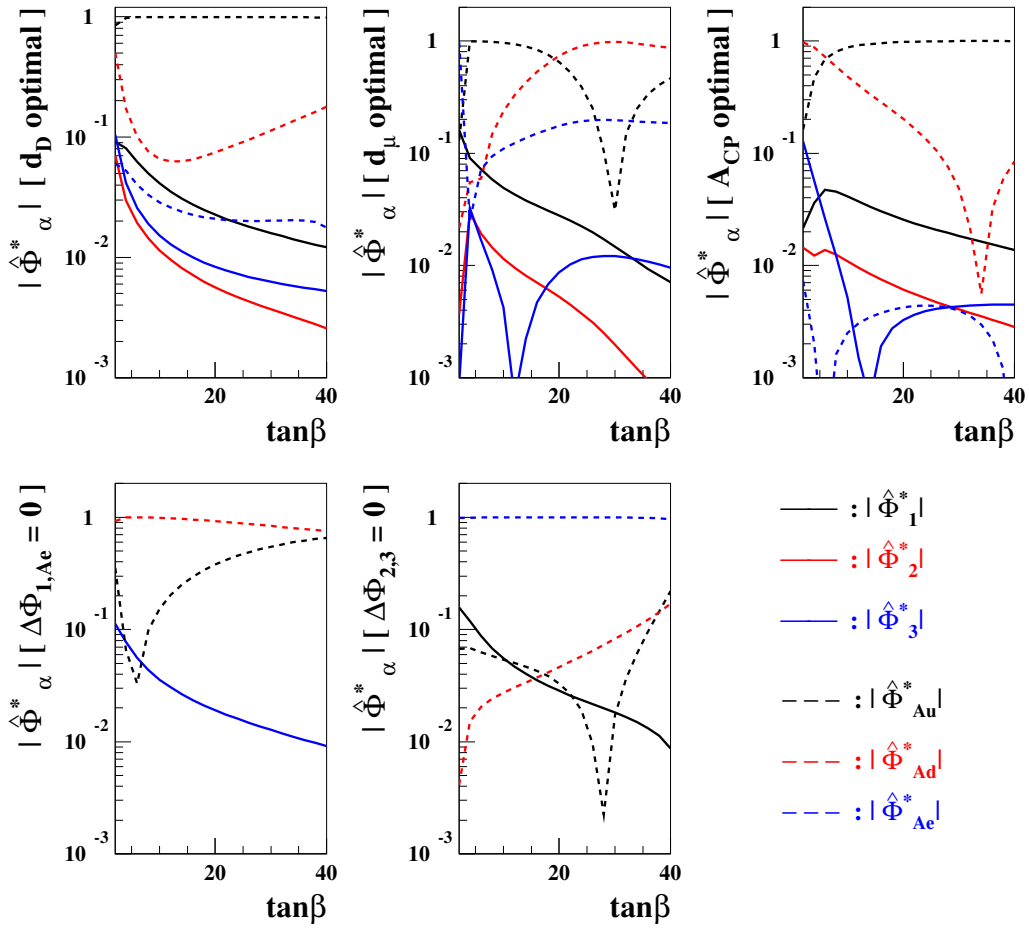

Figure 6. The absolute values of the six components of the five normalized direction vectors considered in the text for $\widetilde{\varphi}_\alpha = 0°$. The solid lines represent the $\Phi_{1,2,3}$ components, and the dashed lines the Φ_{A_u,A_d,A_e} components.

Finally, we consider the products $\widehat{\Phi}^* \cdot \mathbf{O}$ of the 6D vectors of the normalized optimal directions and the observables. The products determine the sizes of the observables along the directions through the relations given in eq. (2.8) when $\phi^* = 1$. As we see in the next section, ϕ^* could be as large as ~ 100 before the small-phase approximation breaks down and one of the three EDM constraints is violated. We show in figure 8 the products for the directions optimized for $d_{\rm D}$, d_μ and $A_{\rm CP}$, which are denoted by the thick black solid, red dashed, and blue dotted lines, respectively. The thin lines are for the products along the reference $\Delta\Phi_{1,A_e} = 0$ (thin black) and $\Delta\Phi_{2,3} = 0$ (thin magenta) directions. The upper frames are for $\widetilde{\varphi}_\alpha = 0°$ and the lower ones for $\widetilde{\varphi}_\alpha = 180°$. We observe that the directions constructed using the geometric prescription given in the previous section do indeed give the optimal values of the observables, which are larger than those along the other optimal and reference directions, sometimes even much larger, depending on $\tan\beta$.

JHEP10(2010)049

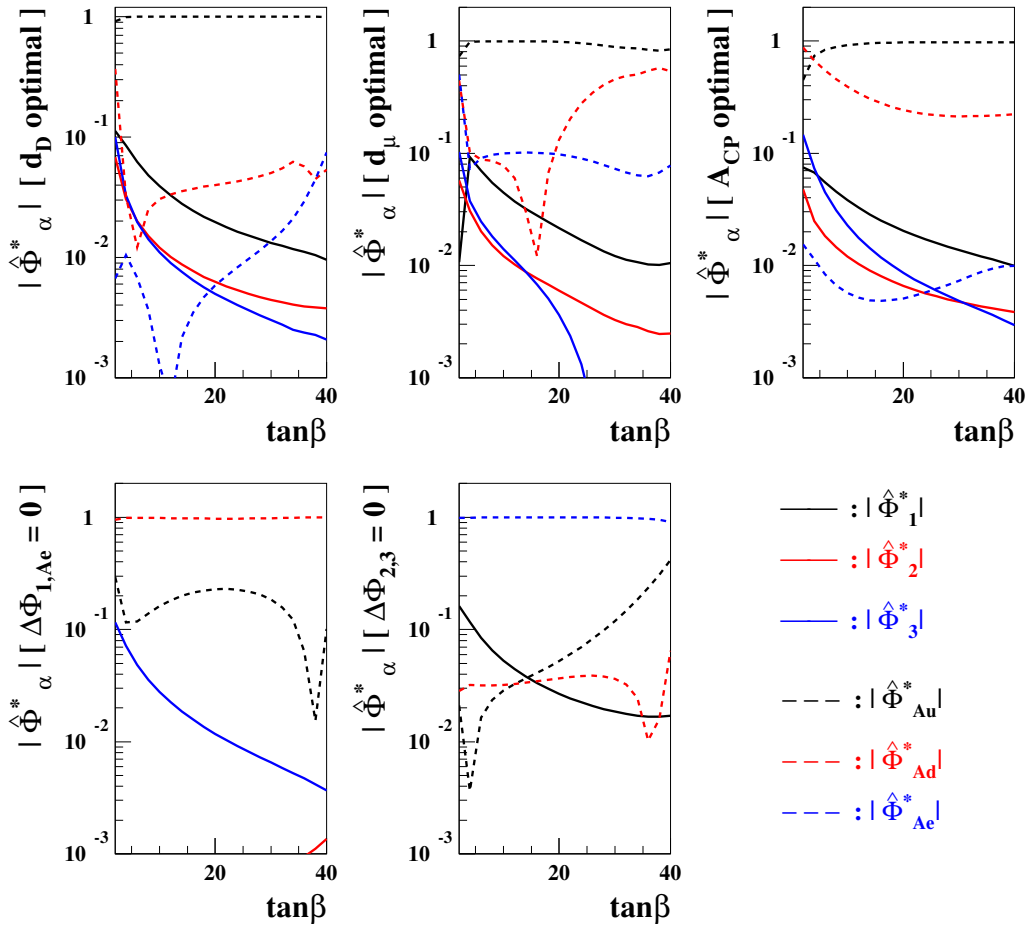

Figure 7. The same as in figure 6, but for $\widetilde{\varphi}_\alpha = 180°$.

4 Optimal values of CP-violating observables in the MCPMFV SUSY model

As preparation for presenting our numerical results for $d_{\rm D}$, d_μ, and $A_{\rm CP}$, we first examine the magnitudes of the Thallium, neutron and Mercury EDMs along the three optimal and two reference directions considered in the previous section. As long as the small-phase approximation is valid, the EDMs should lie below the current experimental limits, but the approximation breaks down for large phases, leading to non-vanishing EDMs larger than the limits. The breakdown of the small-phase approximation would limit the maximum values of ϕ^* in eq. (2.8) to values depending on the choice of direction and, accordingly, limit the maximum values of the CP-odd observables that can be found in this approach.

Figure 9 shows the three constrained EDMs for $\tan\beta = 40$. From this figure, one can read off the maximum allowed value of ϕ^* for each direction. For example, from the upper frames with $\widetilde{\varphi} = 0°$, $(\phi^*)^{\rm max} \sim 70\,, 50\,, 70\,, 50\,,$ and 50 for the $d_{\rm D}$-optimal, d_μ-optimal, $A_{\rm CP}$-optimal, $\Delta\Phi_{1,A_e} = 0$, and $\Delta\Phi_{2,3} = 0$ directions, respectively, with the most important constraints being those provided by $d_{\rm Hg}$, $d_{\rm Hg}$, $d_{\rm Hg}$, $d_{\rm Hg}$, and $d_{\rm Tl}$, respectively. Inserting the

JHEP10(2010)049

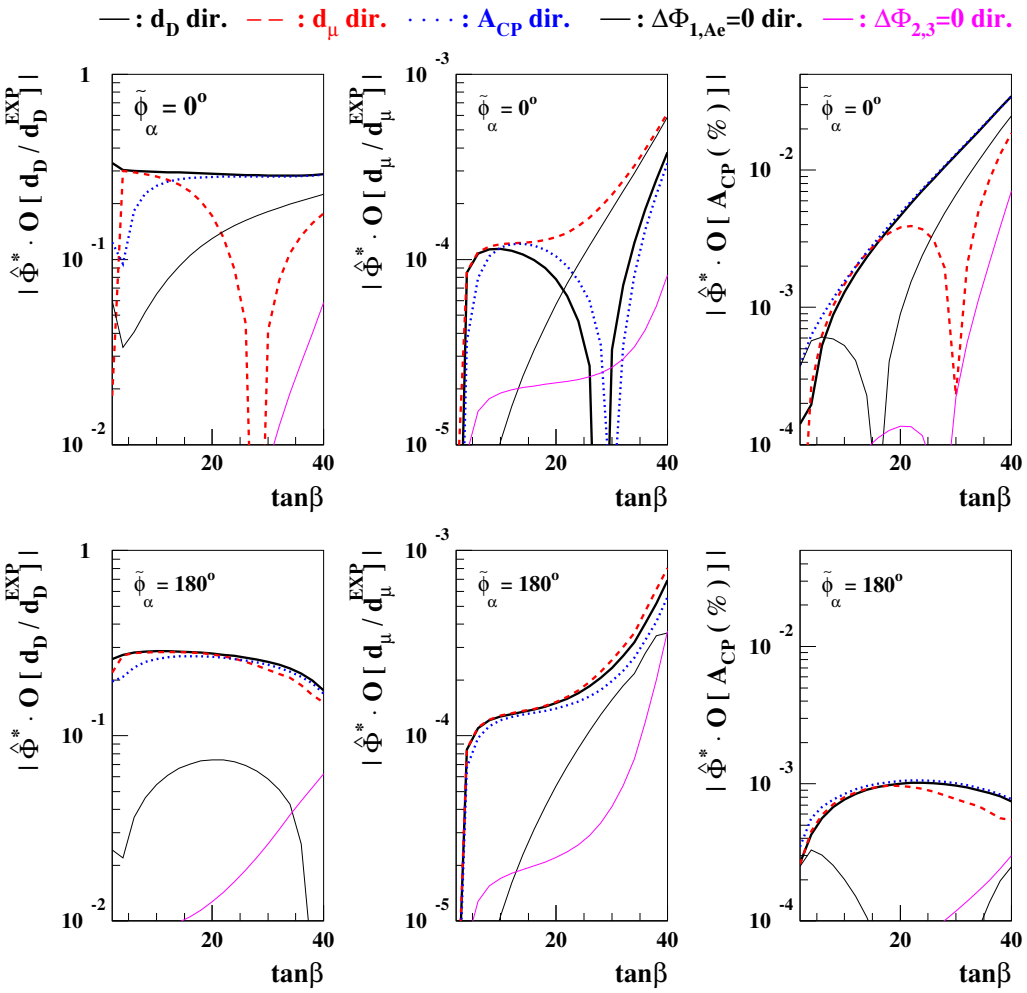

Figure 8. The products $\widehat{\Phi}^* \cdot \mathbf{O}$ along the directions optimized for $d_{\rm D}$, d_μ and $A_{\rm CP}$, which are denoted by the thick black solid, red dashed and blue dotted lines, respectively. The thin lines are for the products along the $\Delta\Phi_{1,A_e} = 0$ (thin black) and $\Delta\Phi_{2,3} = 0$ (thin magenta) directions. The upper frames are for $\widetilde{\varphi}_\alpha = 0°$ and the lower ones for $\widetilde{\varphi}_\alpha = 180°$.

values $(\phi^*)^{\rm max}$ into the corresponding products $\widehat{\Phi}^* \cdot \mathbf{O}$, one may get (near-)maximal values of the CP-odd observables in the linear regime.

Figure 10 shows the three CP-odd observables along the five directions when $\tan\beta = 40$. The experimental upper bounds on the Thallium, neutron and Mercury EDMs have been imposed. In the case of the Deuteron EDM with $\widetilde{\varphi}_\alpha = 0°$, the linear regime ends at $\phi^* \sim \pm 30$, and beyond this range it reaches saturation at a value $\sim |9|$, subsequently decreasing until the maximal value of the angle $(\phi^*)^{\rm max}_{\widetilde{\varphi}_\alpha = 0°} \sim |70|$ is reached. When $\widetilde{\varphi}_\alpha = 180°$, the linear regime ends at $\phi^* \sim \pm 30$. Beyond this point, the Deuteron EDM along the $d_{\rm D}$ optimal direction saturates, but it continues to increase up to $\sim |6|$ along the d_μ and $\Delta\Phi_{1,A_e} = 0$ directions. *These two examples demonstrate that the existing EDM constraints do not exclude the observation of* $d_{\rm D}$.

On the other hand, the muon EDM is always below the projected sensitivity, since

JHEP10(2010)049

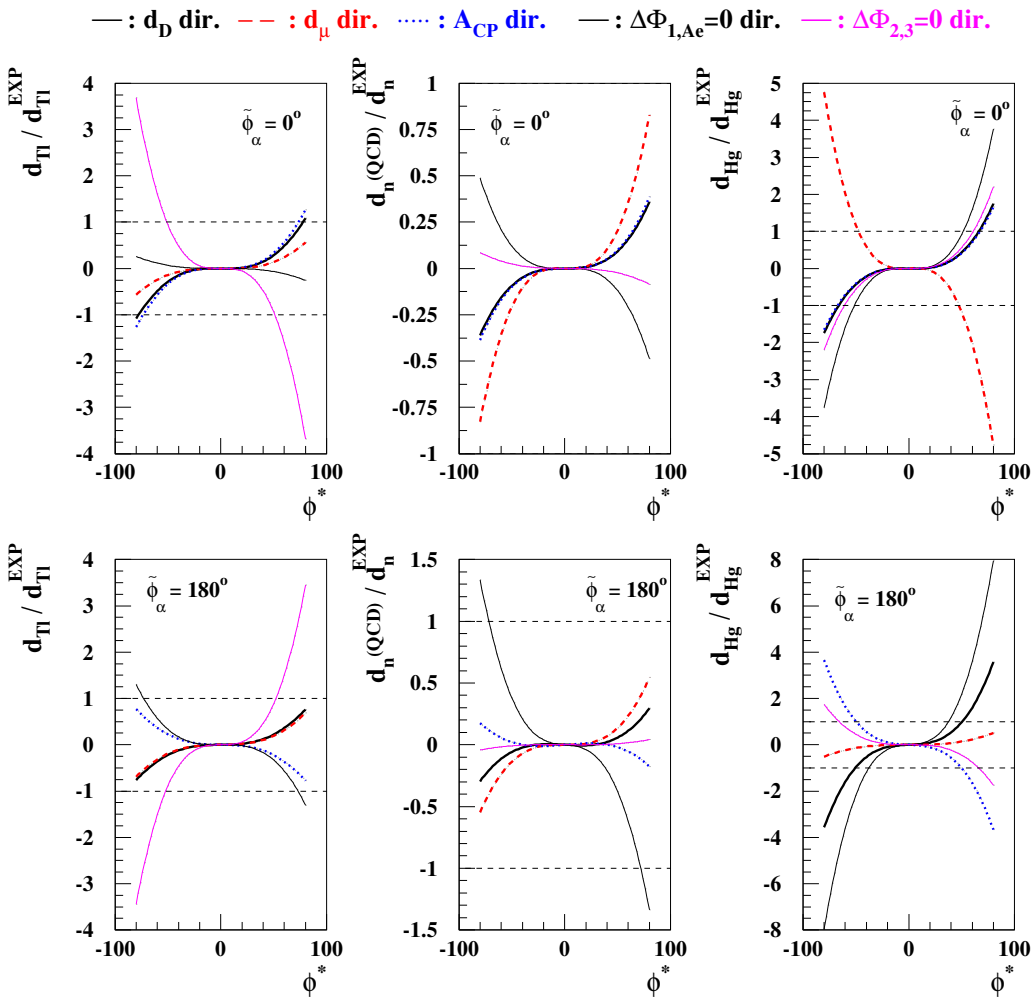

Figure 9. The values of the three EDMs along the three optimal and two reference directions for $\tan\beta = 40$, with $\widetilde{\varphi} = 0°$ (upper) and $\widetilde{\varphi} = 180°$ (upper). The line styles are the same as in figure 8, with the additional horizontal lines representing the EDM constraints.

$\widehat{\Phi}^* \cdot \mathbf{O}^{d_\mu}$ is forced to be small by the (near-) degeneracy with the Thallium EDM, see figure 8.

The CP asymmetry $A_{\rm CP}(b \to s\gamma)$ has a larger linear regime, extending over the almost whole range with $|\phi^*| \lesssim 100$, and could as large as $\sim 2\%$ when $\widetilde{\varphi} = 0°$. Such a value could be observed at a future Super B Factory [40]. Unfortunately, the case with $\tan\beta \sim 40$ gives too small a branching ratio $B(b \to s\gamma) \sim 1 \times 10^{-4}$.[5] In order to respect the constraint from $B(b \to s\gamma)$, we consider the case of small $\tan\beta = 10$ with $\widetilde{\varphi} = 0°$, see figure 11. This case is compatible with the $B(b \to s\gamma)$ constraint at the 2-σ level, but the predicted $A_{\rm CP}$ is too small to be observed. On the other hand, the attainable values of $d_{\rm D}$ and d_μ are similar to those in the case when $\tan\beta = 40$.

Finally, we show in figure 12 the 6 CP-violating phases at the GUT scale and the 3

[5] See also [16], in which the same scenario has been analyzed.

JHEP10(2010)049

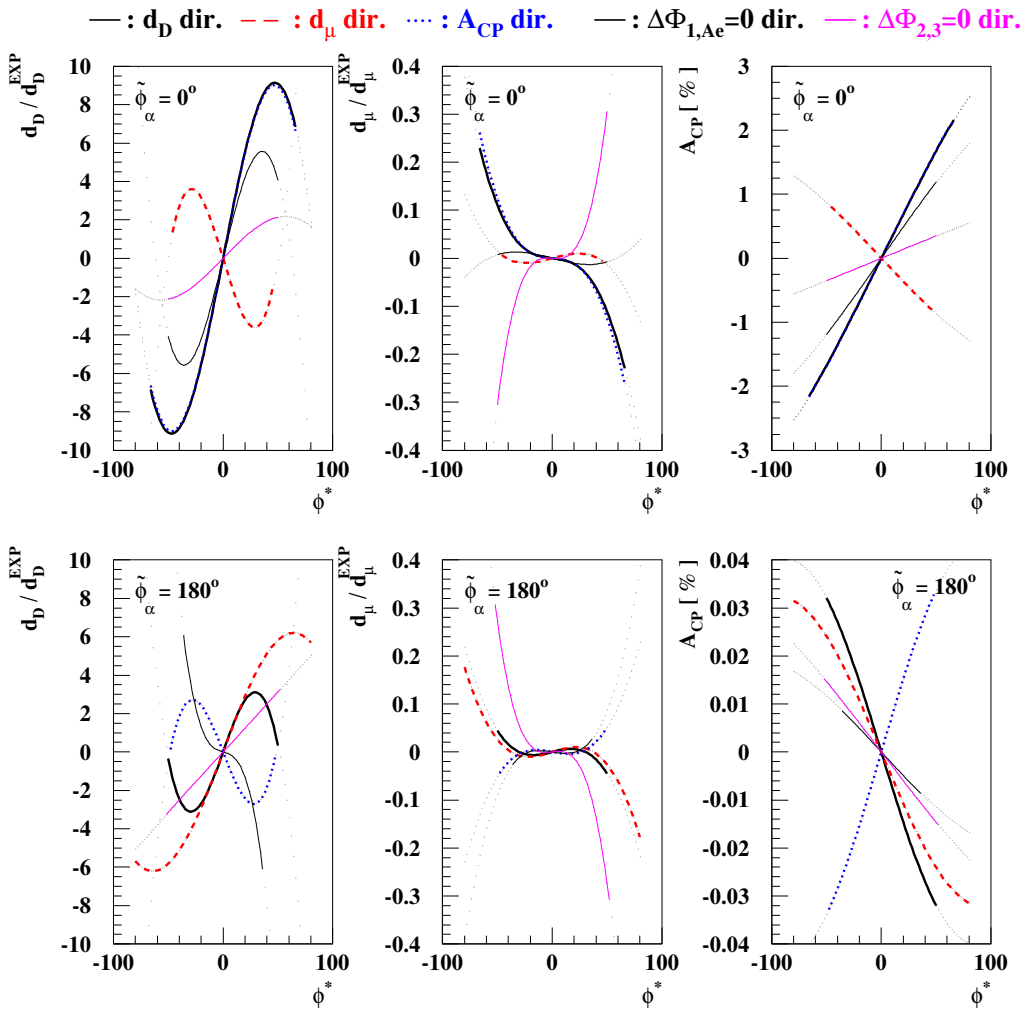

Figure 10. The three CP-odd observables along the three optimal and two reference directions for $\tan\beta = 40$, with $\widetilde{\varphi} = 0°$ (upper) and $\widetilde{\varphi} = 180°$ (upper). The line styles are the same as in figure 8.

CP-violating phases of the third-generation A parameters at the SUSY scale when $\widetilde{\varphi}_\alpha = 0°$ and $\tan\beta = 10$. We observe that the CP-odd gaugino phases Φ_1, Φ_2 and Φ_3 can only be as large as 4°, 1° and 2°, respectively, whereas the CP-odd trilinear A-phases Φ_{A_u,A_d,A_e} at the GUT scale can be as large as ±70°. These CP-violating phases are suppressed at the SUSY scale by RG running from the GUT scale [16], but sizeable non-trivial CP-violating phases are still allowed at the SUSY scale: $\Delta\Phi_{A_t} \sim \pm 4°$, $\Delta\Phi_{A_b} \sim \pm 10°$, and $\Delta\Phi_{A_\tau} \sim \pm 40°$. Similar magnitudes of the CP-violating phases are attainable for $\widetilde{\varphi}_\alpha = 180°$.

5 The 7D extension including $\theta_{\rm QCD}$

In the previous sections, we implicitly assumed that the CP-violating QCD θ-term:

$$\mathcal{L} = \frac{\alpha_s}{8\pi}\,\bar{\theta}\,G^a_{\mu\nu}\tilde{G}^{\mu\nu,a} \tag{5.1}$$

JHEP10(2010)049

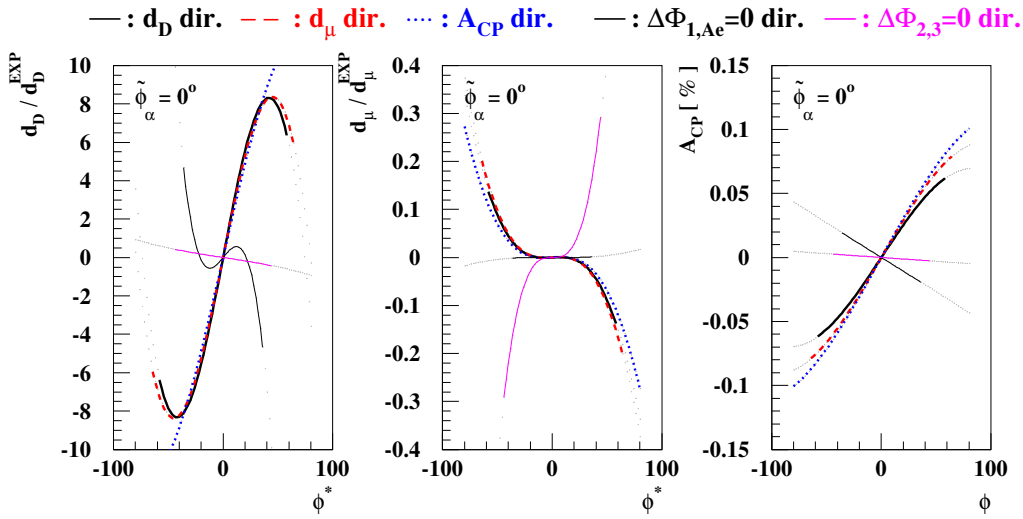

Figure 11. The same as in figure 10, but for $\tan\beta = 10$ and $\widetilde{\varphi} = 0°$.

vanishes, where $\tilde{G}^{\mu\nu,a} = \epsilon^{\mu\nu\rho\sigma} G^a_{\rho\sigma}/2$ and the parameter $\bar{\theta}$ is given by the sum of the QCD $\theta_{\rm QCD}$ and the strong chiral phase for the quark mass matrix as

$$\bar{\theta} = \theta_{\rm QCD} + \mathrm{Arg\,Det}\, M_q\,. \tag{5.2}$$

In the weak basis where $\mathrm{Arg\,Det}\, M_q = 0$, we have $\bar{\theta} = \theta_{\rm QCD}$. The QCD θ-term (5.1) would be set to zero, e.g., if there is a QCD axion in the theory. Otherwise, the dimension-four operator (5.1) would in general contribute to the neutron, Mercury and Deuteron EDMs, e.g., through the CP-odd pion-nucleon-nucleon interactions

$$\mathcal{L}_{\pi NN} = \bar{g}^{(0)}_{\pi NN}\, \overline{N}\tau^a N\, \pi^a \;+\; \bar{g}^{(1)}_{\pi NN}\, \overline{N} N\, \pi^0\,. \tag{5.3}$$

QCD sum rule techniques have been used to estimate the contribution of the $\bar{\theta}$ term to the neutron EDM in [41, 42]:[6]

$$\begin{aligned} d_n(\bar{\theta}) &= (0.4 \pm 0.2)\left[\chi(4e_d - e_u) m_*\, \bar{\theta}\right] \\ &= (1 \pm 0.5) \frac{|\langle \bar{q} q\rangle|}{(225\ \mathrm{MeV})^3}\, \bar{\theta} \times 2.5 \times 10^{-16}\, e\,\mathrm{cm}, \end{aligned} \tag{5.4}$$

where the reduced mass $m_* = m_u m_d/(m_u + m_d)$, $e_d = -(1/3)\,e$, $e_u = (2/3)\,e$, and the condensate susceptibility $\chi = -5.7 \pm 0.6\ \mathrm{GeV}^{-2}$.[7] The $d_n(\bar{\theta})$ contribution is to be added to the other EDM contributions from the electric and chromoelectric dipole moments of light quarks, the Weinberg operators, and the CP-odd four-fermion interactions that are induced

[6] Though there are some inconsistencies between the two references, the second numerical equation in [42] is not affected by them.

[7] It has been argued that, in the presence of an axion, $\bar{\theta}$ should be replaced by $\theta_{\rm ind}$, which is determined dynamically via the chromoelectric dipole moments of the up, down, and strange quarks $d^C_{u,d,s}$. However, since we lack full knowledge of all the relevant higher-order corrections [43], we will neglect $\theta_{\rm ind}$ contributions to EDMs in our analysis.

JHEP10(2010)049

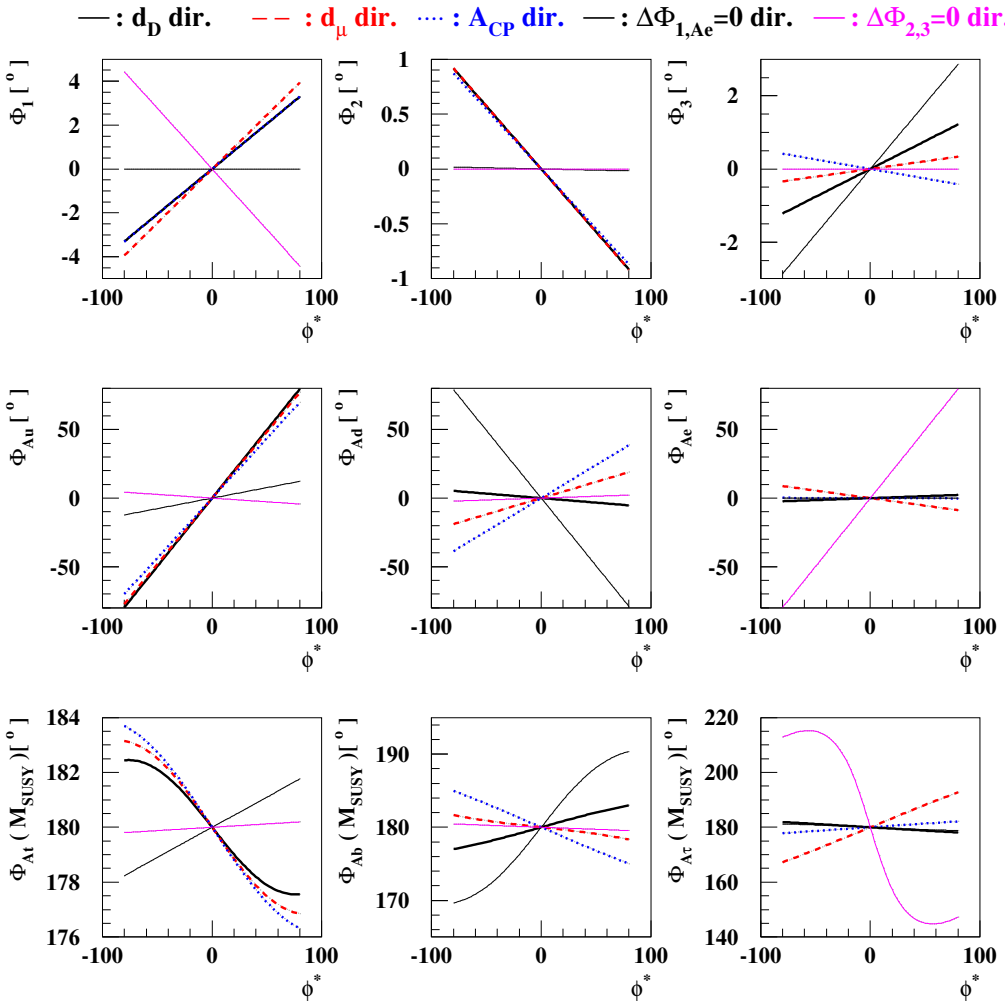

Figure 12. The 6 CP-violating phases at the GUT scale and the 3 CP-violating phases of the third-generation A parameters at the SUSY scale along the 3 EDM-free directions and 2 reference directions when $\widetilde{\varphi}_\alpha = 0°$ and $\tan\beta = 10$.

by the CP-violating phases in the soft SUSY-breaking sector, i.e., by the six independent MCPMFV CP phases considered above [32].

The leading contribution of the $\bar{\theta}$ term to the Mercury EDM is expected to be through its contribution to the pion-nucleon-nucleon interaction coefficient $\bar{g}^{(1)}_{\pi NN}$:

$$d_{\rm Hg}(\bar{\theta}) = +(1.8\times 10^{-3}\,{\rm GeV}^{-1})\, e\, \bar{g}^{(1)}_{\pi NN}(\bar{\theta})\,. \tag{5.5}$$

The $\bar{\theta}$ contribution to the coupling is suppressed by the factor $(m_d - m_u)/m_s$, and given by [15]

$$\bar{g}^{(1)}_{\pi NN}(\bar{\theta}) = \frac{m_*\,\bar{\theta}}{f_\pi}\,\frac{m_d - m_u}{4m_s}\langle N|\bar{u}u + \bar{d}d - 2\bar{s}s|N\rangle \simeq 1.1\times 10^{-3}\,\bar{\theta}\,, \tag{5.6}$$

which results in

$$d_{\rm Hg}(\bar{\theta}) \simeq +2.0\times 10^{-6}\,\bar{\theta}\, e\,{\rm GeV}^{-1} \simeq 3.9\times 10^{-20}\,\bar{\theta}\, e\,{\rm cm}\,. \tag{5.7}$$

JHEP10(2010)049

The leading contributions of the $\bar{\theta}$ term to the Deuteron EDM are given by [15]

$$d_D(\bar{\theta}) \simeq -e\,[(3.5 \pm 1.4) + (1.4 \pm 0.4)] \times 10^{-3}\,\bar{\theta}\,\mathrm{GeV}^{-1} \simeq -9.7 \times 10^{-17}\,\bar{\theta}\,e\,\mathrm{cm}\,. \quad (5.8)$$

The first term is the leading-order QCD sum-rule estimate of the $\bar{\theta}$ contribution to the sum of the proton and neutron EDMs, which enters only via subleading isospin-violating corrections. The second term arises from the coupling $\bar{g}^{(1)}_{\pi NN}(\bar{\theta})$:

$$d_{\mathrm{D}}^{\pi NN}(\bar{\theta}) = -\frac{e\,g_{\pi NN}\,\bar{g}^{(1)}_{\pi NN}(\bar{\theta})}{12\pi m_\pi}\,\frac{1+\xi}{(1+2\xi)^2} \;\simeq\; -(1.3 \pm 0.3)\,e\,\bar{g}^{(1)}_{\pi NN}\,\mathrm{GeV}^{-1}\,, \quad (5.9)$$

where $g_{\pi NN} \simeq 13.45$ and $\xi = \sqrt{m_p \epsilon}/m_\pi$, with $\epsilon = 2.23$ MeV being the Deuteron binding energy.

Including non-vanishing $\bar{\theta}$ together with the six MCPMFV CP phases $\Phi_{1,2,3}$ and Φ_{A_u,A_d,A_e}, there is a total of seven CP phases. The six-dimensional geometric construction of optimal EDM-free directions in section 2 can easily be extended by one more dimension in this case. As in the 6D case, the 7D EDM-constraint and observable vectors are given by $\mathbf{E} = \nabla E$ and $\mathbf{O} = \nabla O$, but with

$$\nabla_\alpha \equiv \left(\frac{\partial}{\partial\Phi_1}, \frac{\partial}{\partial\Phi_2}, \frac{\partial}{\partial\Phi_3}, \frac{\partial}{\partial\Phi_{A_u}}, \frac{\partial}{\partial\Phi_{A_d}}, \frac{\partial}{\partial\Phi_{A_e}}, \frac{\partial}{\partial\widehat{\theta}}\right)\,. \quad (5.10)$$

As before the CP-violating phases $\Phi_{1,2,3}$ and Φ_{A_u,A_d,A_e} are specified in degrees and we normalize $\bar{\theta}$ in units of 10^{-10}:

$$\widehat{\theta} \equiv \bar{\theta} \times 10^{10}\,. \quad (5.11)$$

With this normalization, with $\widehat{\theta} = 1$, we have $d_n(\bar{\theta}) = 2.5 \times 10^{-26}\,e\,\mathrm{cm}$ which is very near to the current experimental bound $d_n^{\mathrm{EXP}} = 3 \times 10^{-26}\,e\,\mathrm{cm}$.

In figure 13, we show the absolute values of the components of the three 7D EDM-constraint and the three 7D observable vectors in the linearized CP-violating version of the scenario (3.1), taking $\widetilde{\varphi}_{\alpha=1-6} = 0°$. Comparing with figure 3 of the 6D case, we see that: (i) $\mathbf{E}^{d_{\mathrm{Tl}}}$, $\mathbf{O}^{d_\mu}$, and $\mathbf{O}^{A_{\mathrm{CP}}}$ are unchanged, with vanishing seventh $\widehat{\theta}$ components, (ii) the first six components of $\mathbf{E}^{d_{\mathrm{n}}}$, $\mathbf{E}^{d_{\mathrm{Hg}}}$ and $\mathbf{O}^{d_{\mathrm{D}}}$ are unchanged, and we have the new $\widehat{\theta}$ components, $\left(\mathbf{E}^{d_{\mathrm{n}}}\right)_7 \simeq 0.83$, $\left(\mathbf{E}^{d_{\mathrm{Hg}}}\right)_7 \simeq 0.13$ and $\left(\mathbf{E}^{d_{\mathrm{D}}}\right)_7 \simeq -3.2$, which are independent of $\tan\beta$.

Having obtained the 7D $\mathbf{E}$ and $\mathbf{O}$ vectors, one can construct the optimal EDM-free direction maximizing O as in the 6D case:

$$\Phi^*_\alpha \;=\; \mathcal{N}\,\varepsilon_{\alpha\beta\gamma\delta\mu\nu\rho}\,E^{d_{\mathrm{Tl}}}_\beta\,E^{d_{\mathrm{n}}}_\gamma\,E^{d_{\mathrm{Hg}}}_\delta\,B_{\mu\nu\rho}\,, \quad (5.12)$$

where the 3-form $B_{\mu\nu\rho}$ is given by

$$B_{\mu\nu\rho} \;=\; \varepsilon_{\mu\nu\rho\lambda\sigma\tau\omega}\,O_\lambda\,E^{d_{\mathrm{Tl}}}_\sigma\,E^{d_{\mathrm{n}}}_\tau\,E^{d_{\mathrm{Hg}}}_\omega\,. \quad (5.13)$$

We show in figure 14 the absolute values of the seven components of the three optimum directions (upper) and the two reference directions with $\Delta\Phi_1 = \Delta\Phi_{A_e} = \widehat{\theta} = 0$ (lower left) and $\Delta\Phi_2 = \Delta\Phi_3 = \widehat{\theta} = 0$ (lower middle), considering the scenario (3.1) with $\widetilde{\varphi}_{\alpha=1-6} =$

JHEP10(2010)049

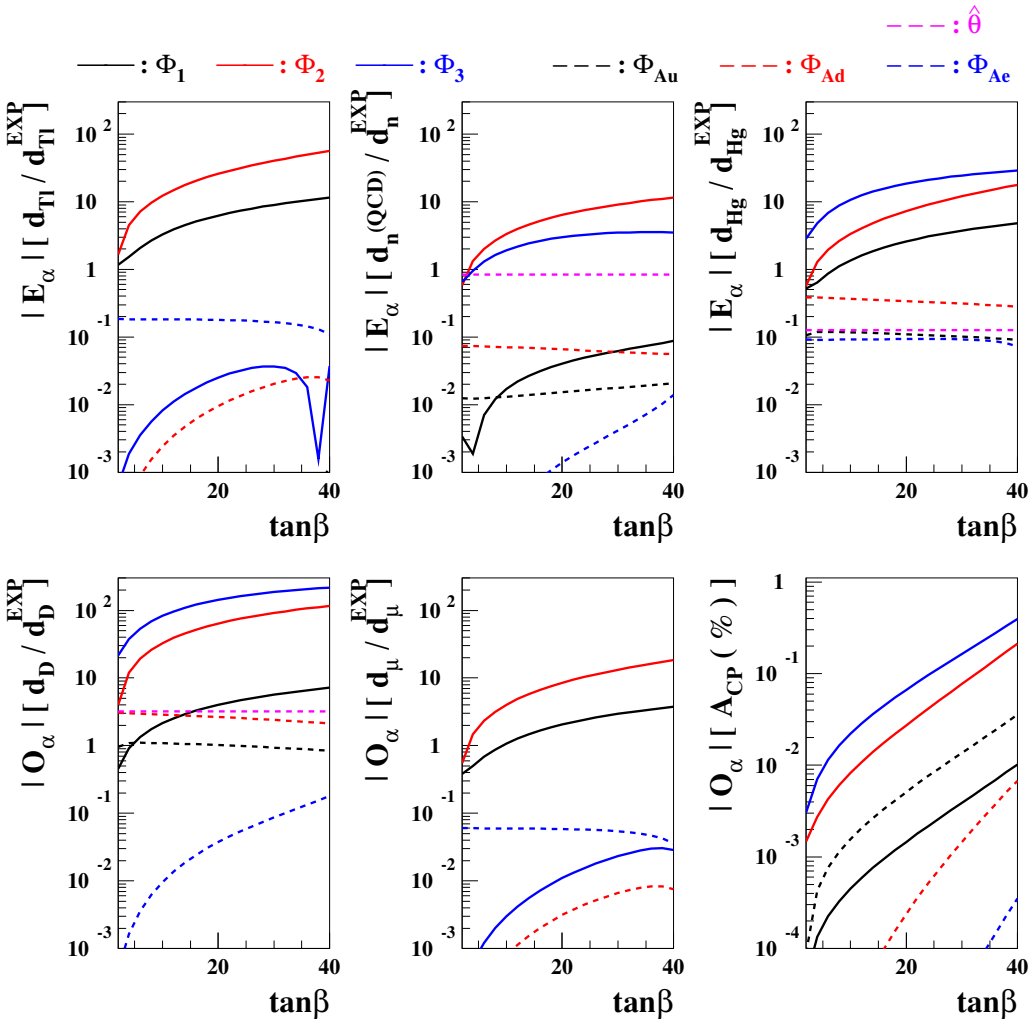

Figure 13. The absolute values of the components of the three 7D EDM-constraint vectors (upper) and those of the three 7D observable vectors (lower) in linear expansions around $\widetilde{\varphi}_{\alpha=1-6} = 0°$, as functions of $\tan\beta$ for the scenario (3.1). The magenta dashed lines represent the $\widehat{\theta} = \bar{\theta} \times 10^{10}$ component, while the other lines are the same as in figure 3.

0°. Comparing with figure 6 of the 6D case, we see that: (*i*) the vectors in the two reference directions with $\widehat{\theta} = 0$ remain the same, (*ii*) the $d_{\rm D}$- and d_μ-optimal directions can now have sizeable $\Phi_{1,2}$ components, while the $\widehat{\theta}$ component dominates when $\tan\beta \gtrsim 10$, (*iii*) the $A_{\rm CP}$-optimal direction is still dominated by the Φ_{A_u} component when $\tan\beta \gtrsim 7$. Figure 15 shows the products with the three observable vectors of the three optimal EDM-free directions and the two reference directions for the same scenario. We observe again that the optimal direction found using our geometric construction gives the largest value for each corresponding observable. Comparing with figure 8 (upper frames) of the 6D case, the products can be larger by more than an order of magnitude for the Deuteron and muon EDMs. On the other hand, they remain more or less the same for $A_{\rm CP}$, due to the dominance of the Φ_{A_u} component in the $A_{\rm CP}$-optimal direction.

JHEP10(2010)049

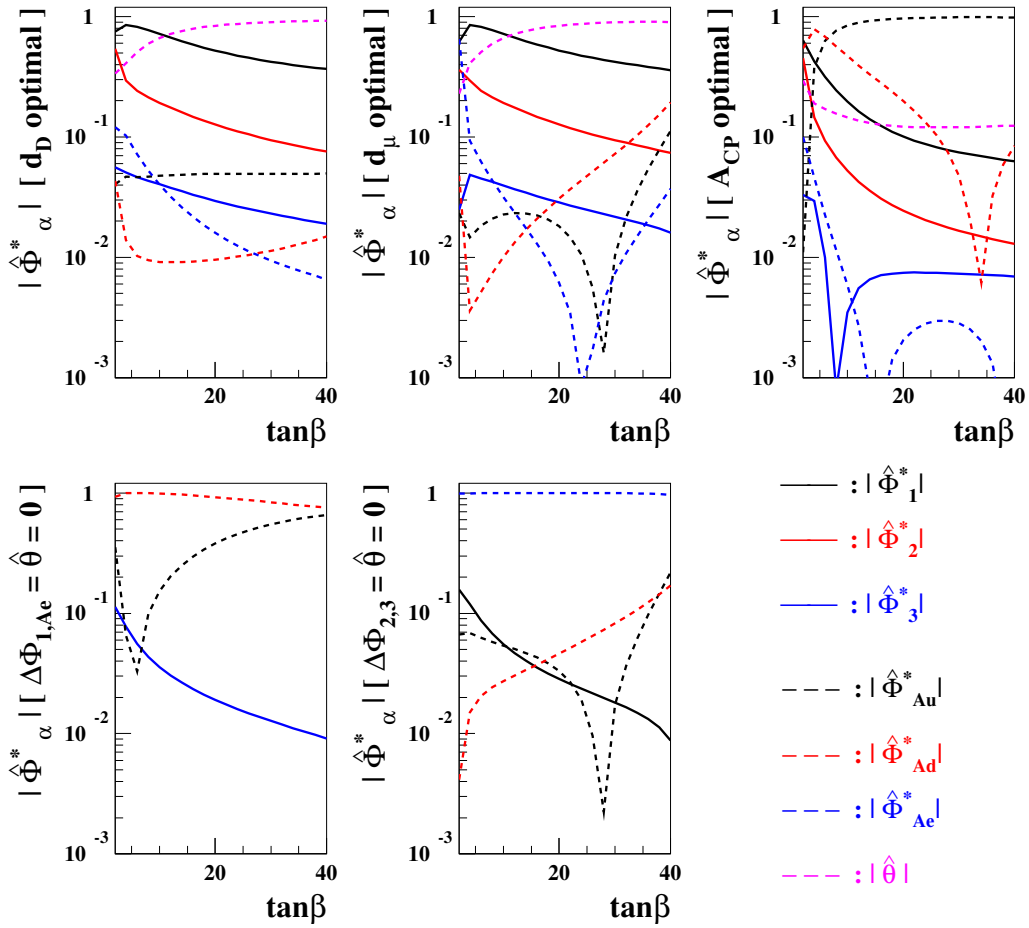

Figure 14. The absolute values of the seven components of the five normalized direction vectors for the 7D CP-violating version of the scenario (3.1), in a linear expansion around $\widetilde{\varphi}_{\alpha=1-6} = 0°$. The lines are the same as in figure 6, with additional magenta lines for the $\widehat{\theta}$ components.

In the upper frames of figure 16, we show the three EDM constraints, assuming $\tan\beta = 10$ and $\widetilde{\varphi}_{\alpha=1-6} = 0°$. As in the case of figure 9, one can read off the maximum values of ϕ^* for each EDM-free direction from the figure: $(\phi^*)^{\max} \sim 25\,, 25\,, 50\,, 40\,,$ and 45 for the $d_{\rm D}$-optimal, d_μ-optimal, $A_{\rm CP}$-optimal, $\Delta\Phi_{1,A_e} = \widehat{\theta} = 0$, and $\Delta\Phi_{2,3} = \widehat{\theta} = 0$ directions, which are mainly constrained by $d_{\rm Tl}$, $d_{\rm Tl}$, $d_{\rm Tl}$, $d_{\rm Hg}$, and $d_{\rm Tl}$, respectively. Multiplying the values $(\phi^*)^{\max}$ to the corresponding products $\widehat{\Phi}^* \cdot \mathbf{O}$ shown in figure 15, we find the maximum values of the CP-odd observables in the linear regime, which are shown in the lower frames of figure 16. Comparing with figure 11 of the 6D case, we see that the maximal value of the Deuteron EDM is greatly enhanced, becoming as large as ~ 70 times the projected sensitivity. On the other hand, the muon EDM is still below the projected sensitivity, and the the maximal value of the CP asymmetry $A_{\rm CP}(b \to s\gamma)$ could be only $\sim 0.08\%$.

Finally, in figure 17, we show the 6 CP-violating phases at the GUT scale and the 3 CP phases of the third-generation A parameters at the SUSY scale along the 3 EDM-free and the 2 reference directions in the 7D case. Comparing with figure 12 for the 6D case,

JHEP10(2010)049

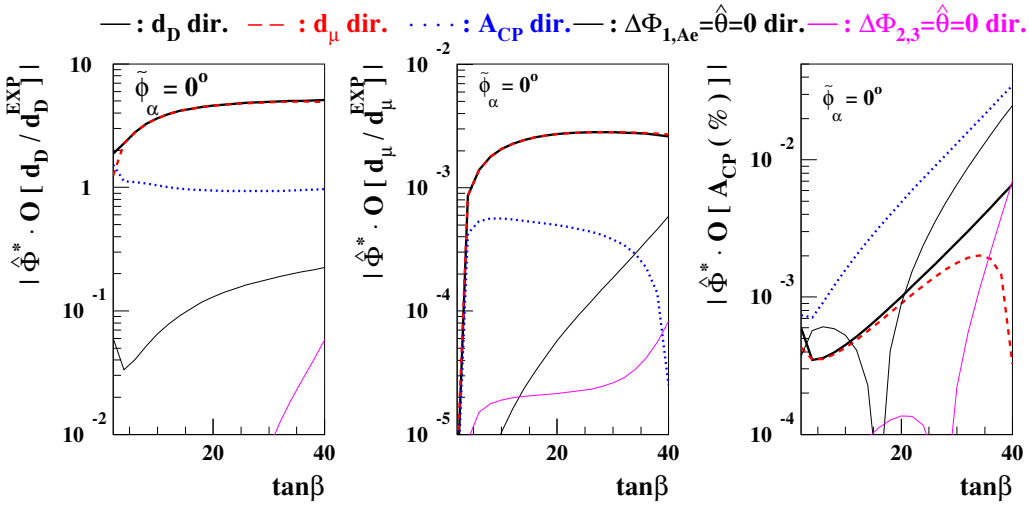

Figure 15. The products $\widehat{\Phi}^* \cdot \mathbf{O}$ along the three $d_{\rm D}$-, d_μ-, and $A_{\rm CP}$-optimal and the two arbitrary directions for the 7D CP-violating version of the scenario (3.1) with $\widetilde{\varphi}_{\alpha=1-6} = 0°$. The lines are the same as in figure 8.

we observe in the top panels that Φ_1 and Φ_2 can be substantially larger, as large as $\sim 20°$ and $\sim 5°$, respectively, for $(\phi^*)^{\rm max} \sim 25$ along the $d_{\rm D}$- and d_μ-optimal directions denoted by the thick solid and dashed lines. We also note in the middle and bottom panels that the phases of $A_{d,u,e}$ are somewhat larger than in the 6D case. Finally, we note (not shown) that $\bar{\theta}$ could be as large as $\sim 5 \times 10^{-9}$ along the $A_{\rm CP}$-optimal direction.

6 Conclusions

We have proposed in this paper a novel geometric technique for optimizing the possible values of CP-violating observables in the presence of the strong constraints due to upper limits on EDMs. Our geometric approach enables us to separate the EDM-free subspace off the full CP-phase parameter space in the linear approximation. Knowing the parametric dependence of a given observable, we can *analytically* construct the extremal direction in the full parameter space, along which the observable gets maximized. Since our approach is analytic, it becomes exact in the linear approximation and is much more efficient and accurate than the naive type of scan that is usually made in literature [18, 27–32].[8]

We have demonstrated the applicability of this technique in two cases: the 6D case of the MCPMFV version of the MSSM, and a 7D extension to include the QCD vacuum phase. We have illustrated this approach within a class of CP-violating models that extend and generalize the well-studied SPS1a benchmark point of the CMSSM. For any specific benchmark point, the values of CP-violating observables are in general bounded in magni-

[8]For comparison, we note that, for a theory with 6 free parameters, a search within a 6-dimensional grid with 100 points in each coordinate would require 10^{12} scan points. Instead, our geometric method only involves straightforward sums over a 6-dimensional Levi-Civita tensor with $6! = 720$ non-zero components, along a radial line of 50 points.

JHEP10(2010)049

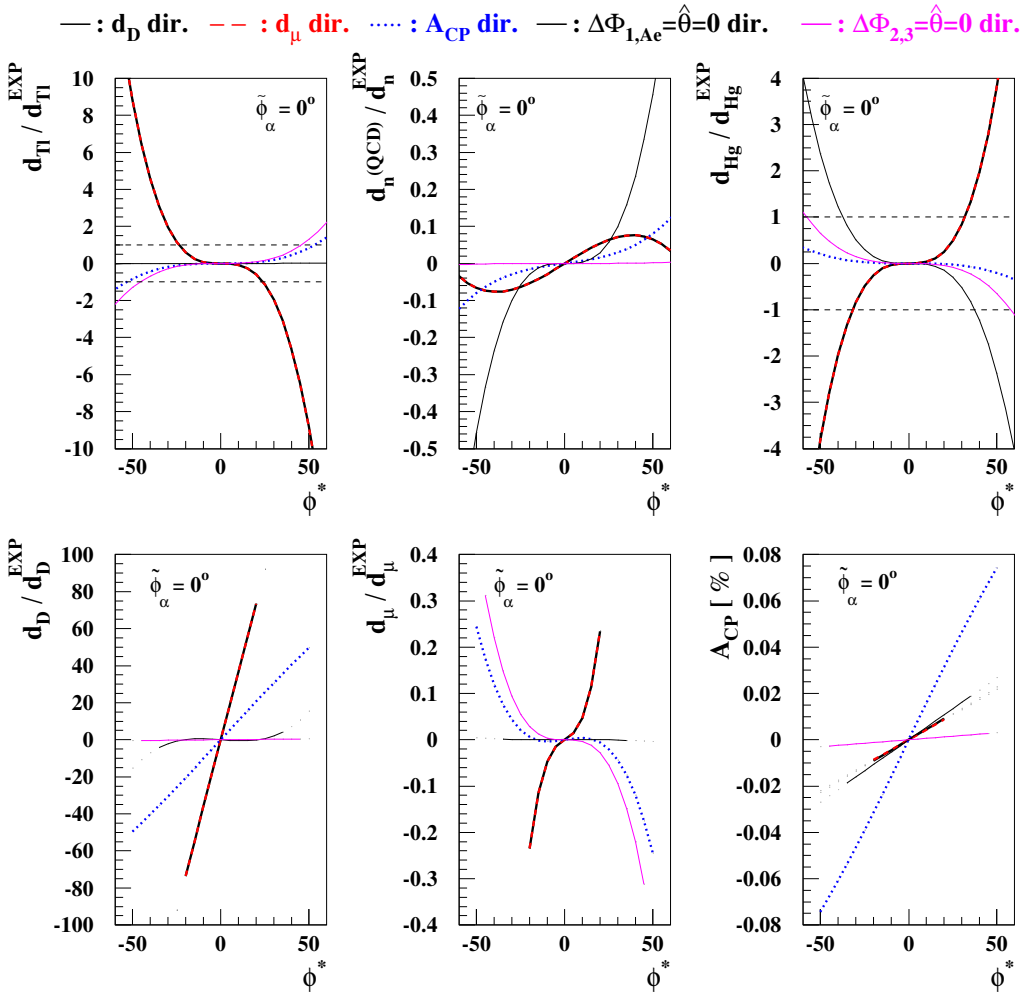

Figure 16. Upper: The three EDM constraints along the three EDM-free and two reference directions for the scenario (3.1) with $\tan\beta = 10$ and $\widetilde{\varphi}_{\alpha=1-6} = 0°$. Lower: The three CP-odd observables in the same scenario. The lines are the same as in figures 9 and 10.

tude, since the ranges of the CP-violating phases ϕ_i are all compact: $\phi_i \in [0, 2\pi)$. Based on linear expansions of CP-violating observables around CP-conserving points with $\phi_i = 0, \pi$, our approach gives rather accurate estimates of the true maximal values of the CP-violating observables.

Using this approach in the 6D MCPMFV case, we find values of the Deuteron EDM that may be an order of magnitude larger than the prospective experimental sensitivity. This range is increased by almost another order of magnitude if our optimal geometric construction is extended to the 7D case that includes the CP-violating QCD vacuum phase. Hence, the Deuteron EDM may provide indirect useful information about the possible presence of a non-vanishing QCD vacuum phase, complementing the current experiments on EDMs and the experimental searches for axions [44, 45]. On the other hand, we find that the maximal values of the muon EDM are somewhat below the likely experimental

JHEP10(2010)049

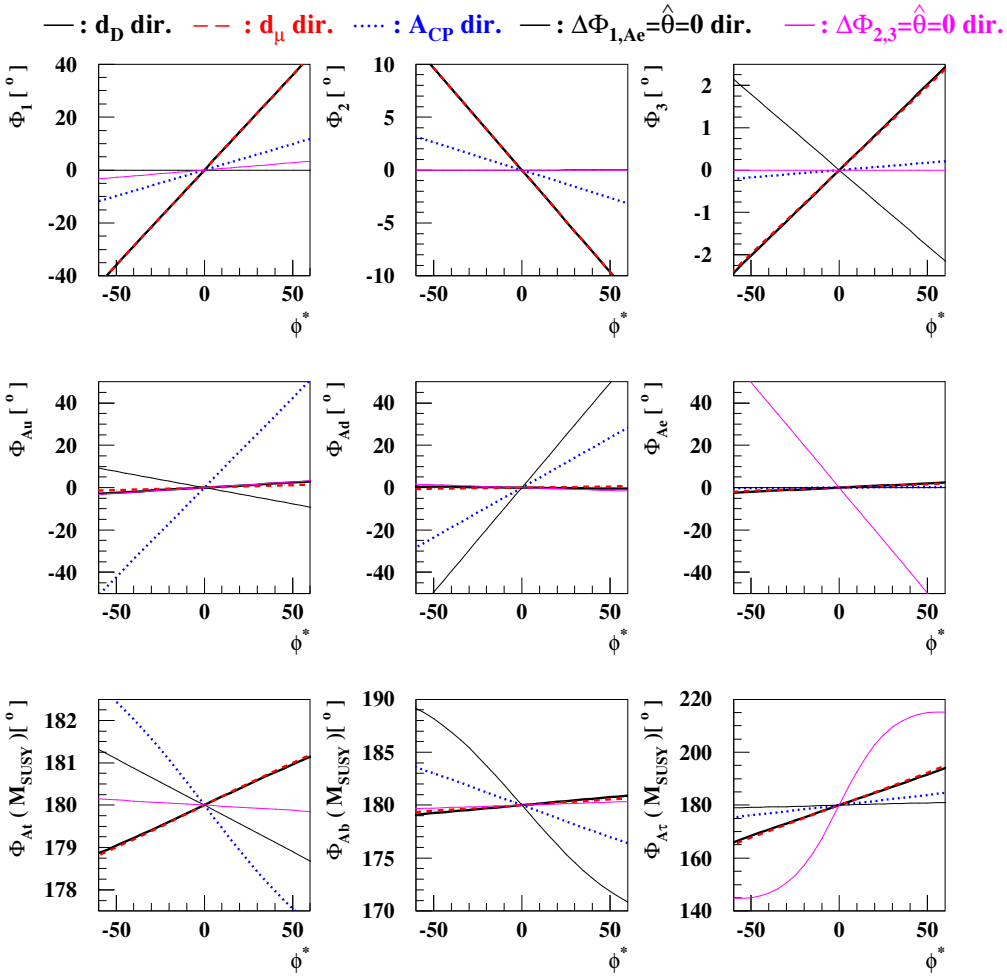

Figure 17. The 6 CP phases at the GUT scale and the 3 CP-violating phases of the third-generation A parameters at the SUSY scale along the 3 EDM-free and 2 reference directions. The scenario (3.1) is taken with $\tan\beta = 10$ and $\widetilde{\varphi}_{\alpha=1-6} = 0°$. The line styles are the same as in figure 12.

sensitivity in both the scenarios with and without the QCD phase. We also find that the CP-violating $b \to s\gamma$ decay asymmetry $A_{\rm CP}$ is too small to be observed, once the stringent constraint from $B(b \to s\gamma)$ is taken into account. Likewise, the B_s-mixing phase ϕ_{B_s} turns out to be close to the small SM value in both the scenarios studied.

Our geometric approach could easily be extended to other supersymmetric scenarios. For example, we have not made a systematic survey of all the possibilities in the MCPMFV SUSY model that arise as generalizations of other CP-conserving benchmarks. It may also be interesting to extend this approach to a wider class of CP-violating models within the general MSSM framework. Since it has many more CP-violating parameters, our approach may be a useful guide to the possibilities opened up by this larger parameter space. Needless to say, our approach may also be interesting for other scenarios for CP violation, beyond the MSSM and indeed supersymmetry. Finally, we observe that this geometric approach is

JHEP10(2010)049

not restricted to issues related only to CP violation. It could find broader applicability to other problems where one wants to maximize observables subject to a set of constraints.

Acknowledgments

We thank Maxim Pospelov, Adam Ritz and We-Fu Chang for helpful discussions. The work of A.P. was supported in part by the STFC research grant PP/D000157/1.

A Two-loop gaugino contributions to EDMs

In this appendix we calculate a particular set of EDM contributions induced by two-loop diagrams involving chargino ($\tilde{\chi}^{\pm}$) and neutralino ($\tilde{\chi}^0$) quantum effects. The relevant tree-level interactions are:

$$\begin{aligned}
\mathcal{L}_{A\bar{f}f} &= -e\,\overline{\tilde{\chi}^+}\gamma^\mu\tilde{\chi}^+\,A_\mu \;=\; +e\,\overline{\tilde{\chi}^-}\gamma^\mu\tilde{\chi}^-\,A_\mu\,, \\
\mathcal{L}_{H^\pm\tilde{\chi}_i^0\tilde{\chi}_j^\mp} &= -\frac{g}{\sqrt{2}}\,H^+\,\overline{\tilde{\chi}_i^0}\left(g^S_{H^+\tilde{\chi}_i^0\tilde{\chi}_j^-}+i\gamma_5\,g^P_{H^+\tilde{\chi}_i^0\tilde{\chi}_j^-}\right)\tilde{\chi}_j^- \;+\; \text{H.c.}\,, \\
\mathcal{L}_{W^\pm\tilde{\chi}_i^0\tilde{\chi}_j^\mp} &= -\frac{g}{\sqrt{2}}\,W_\mu^+\,\overline{\tilde{\chi}_i^0}\,\gamma^\mu\left(g^L_{W^+\tilde{\chi}_i^0\tilde{\chi}_j^-}P_L+g^R_{W^+\tilde{\chi}_i^0\tilde{\chi}_j^-}P_R\right)\tilde{\chi}_j^- \;+\; \text{H.c.}\,,
\end{aligned} \tag{A.1}$$

where the $H^\pm$-boson couplings are given in the `CPsuperH` manual [46, 47], and the $W^\pm$-boson couplings are given by

$$\begin{aligned}
g^L_{W^+\tilde{\chi}_i^0\tilde{\chi}_j^-} &= N_{i3}(C_L)^*_{j2}+\sqrt{2}N_{i2}(C_L)^*_{j1}\,, \\
g^R_{W^+\tilde{\chi}_i^0\tilde{\chi}_j^-} &= -N^*_{i4}(C_R)^*_{j2}+\sqrt{2}N^*_{i2}(C_R)^*_{j1}\,,
\end{aligned} \tag{A.2}$$

in terms of chargino and neutralino mixing matrices. The charged-Higgs couplings to the SM particles are given by

$$\mathcal{L}_{H^\pm ff'} = -g_{ff'}H^+\,\overline{f}\left(g^S_{H^+\bar{f}f'}+i\gamma_5\,g^P_{H^+\bar{f}f'}\right)f' \;+\; \text{H.c.}, \tag{A.3}$$

where

$$g_{\nu l} = -\frac{gm_l}{\sqrt{2}M_W}\,, \qquad g^S_{H^+\bar{\nu}l} = t_\beta/2\,, \qquad g^P_{H^+\bar{\nu}l} = -it_\beta/2\,. \tag{A.4}$$

We include the threshold corrections due to the exchanges of gluinos:

$$\begin{aligned}
g_{ud} &= -\frac{gm_u}{\sqrt{2}M_W}\,, \\
g^S_{H^+\bar{u}d} &= \frac{1}{2}\left(\frac{1}{t_\beta}+\frac{t_\beta}{1+\Delta_d^*\,t_\beta}\,\frac{m_d}{m_u}\right)\,, \\
g^P_{H^+\bar{u}d} &= \frac{i}{2}\left(\frac{1}{t_\beta}-\frac{t_\beta}{1+\Delta_d^*\,t_\beta}\,\frac{m_d}{m_u}\right)\,,
\end{aligned} \tag{A.5}$$

where

$$\Delta_d = \frac{2\alpha_s}{3\pi}\mu^*M_3^*I(M^2_{\tilde{D}},M^2_{\tilde{Q}},|M_3|^2)\,. \tag{A.6}$$

JHEP10(2010)049

We note that this threshold correction induces a dependence on the gluino mass phase Φ_3. At the two-loop level, charginos and neutralinos induce CP-violating interactions in the γ-$H^\pm$-$W^\mp$ and γ-$W^\pm$-$W^\mp$ couplings, which in turn produce non-zero electron and quark EDMs.

A.1 EDM induced by the γ-$H^\pm$-$W^\mp$ coupling

In addition to squarks [48, 49], charginos and neutralinos may also induce a complex and CP-violating effective γ-$H^\pm$-$W^\mp$ coupling [37, 38]. The CP-violating effective γ-$H^\pm$-$W^\mp$ coupling can then give rise to electron and d-quark EDMs. Specifically, defining as $f' \equiv l, d$ all fermions with weak isospin $T_z = -1/2$, we have

$$\begin{aligned}\left(\frac{d^E_{f'}}{e}\right)^{WH^\pm} &= \frac{\alpha^2}{64\pi^2 s_W^4}\left(\frac{-\sqrt{2}\,g_{ff'}}{g}\right)\frac{1}{M^2_{H^\pm}} \\ &\times\sum_{i=1}^{4}\sum_{j=1}^{2}\Bigg\{\int \mathrm{d}x\,\frac{1}{1-x}\,J\left(r_{WH^\pm},\frac{r_{jH^\pm}}{1-x}+\frac{r_{iH^\pm}}{x}\right) \\ &\Bigg[\Im\mathrm{m}\Big((g^S_{H^+\bar f f'}+ig^P_{H^+\bar f f'})\,G^{RL}_{+}\Big)\,m_{\tilde\chi^\pm_j}\,x^2 \\ &+\Im\mathrm{m}\Big((g^S_{H^+\bar f f'}+ig^P_{H^+\bar f f'})\,G^{LR}_{+}\Big)\,m_{\tilde\chi^0_i}\,(1-x)^2 \\ &+\Im\mathrm{m}\Big((g^S_{H^+\bar f f'}+ig^P_{H^+\bar f f'})\,G^{RL}_{-}\Big)\,m_{\tilde\chi^\pm_j}\,x \\ &+\Im\mathrm{m}\Big((g^S_{H^+\bar f f'}+ig^P_{H^+\bar f f'})\,G^{LR}_{-}\Big)\,m_{\tilde\chi^0_i}\,(1-x)\Bigg]\Bigg\}\,, \end{aligned} \tag{A.7}$$

where $r_{xy} \equiv M_x^2/M_y^2$ and

$$\begin{aligned} G^{AB}_{\pm} \equiv &\left(g^S_{H^+\tilde\chi^0_i\tilde\chi^-_j}\right)^*\left(g^A_{W^+\tilde\chi^0_i\tilde\chi^-_j}\pm g^B_{W^+\tilde\chi^0_i\tilde\chi^-_j}\right) \\ &+i\left(g^P_{H^+\tilde\chi^0_i\tilde\chi^-_j}\right)^*\left(g^A_{W^+\tilde\chi^0_i\tilde\chi^-_j}\mp g^B_{W^+\tilde\chi^0_i\tilde\chi^-_j}\right)\,, \end{aligned} \tag{A.8}$$

with $A, B = L, R$. The loop function $J(a,b)$ is defined in terms of the function $J(x)$,

$$J(x) \;\equiv\; \frac{x\ln x}{x-1}\,, \tag{A.9}$$

by $J(a,b) \equiv [J(a) - J(b)]/(a-b)$. For $a = b$, the loop function $J(a,b)$ takes on the simple form: $J(a,a) = (-\ln a + a - 1)/(a-1)^2$, with $J(1,1) = 1/2$. Observe that the expression $g^S_{H^+\bar f f'} + ig^P_{H^+\bar f f'} = t_\beta\,(t_\beta\, m_d/m_u)$ for $f' = l$ (d) is real at the tree level, but becomes in general complex when gluino threshold corrections are included, as discussed above.

A.2 EDM induced by the γ-$W^\pm$-$W^\mp$ coupling

Quantum loops of charginos and neutralinos generate P- and CP-odd interactions in the γ-$W^\pm$-$W^\mp$ coupling [50–53], which in turn produce non-zero fermion EDMs at the two-loop

JHEP10(2010)049

level. The analytic results we use are based on the latest calculation in [53]. In detail, if we define $f \equiv l, d$, the contribution of the γ-$W^{\pm}$-$W^{\mp}$ coupling to the f-particle EDM is given by

$$\left(\frac{d_f^E}{e}\right)^{WW} = \frac{\alpha^2}{32\pi^2 s_W^4} \Im\mathrm{m}\left[g^L_{W^+\tilde{\chi}_i^0\tilde{\chi}_j^-}\left(g^R_{W^+\tilde{\chi}_i^0\tilde{\chi}_j^-}\right)^*\right] \frac{m_f\, m_{\tilde{\chi}_i^0}\, m_{\tilde{\chi}_j^\pm}}{M_W^4}\, f_{WW}(r_i, r_j)\,, \quad \text{(A.10)}$$

where

$$f_{WW}(r_i, r_j) = \int_0^1 \frac{\mathrm{d}x}{1-x}\, J\left(0\,, \frac{(1-x)r_i + x r_j}{x(1-x)}\right)\,, \quad \text{(A.11)}$$

with $r_j \equiv m^2_{\tilde{\chi}_j^\pm}/M_W^2$ and $r_i \equiv m^2_{\tilde{\chi}_i^0}/M_W^2$, and $J(a,b)$ being defined after (A.9).

A.3 `CPsuperH2.2` interface

The additional two-loop EDMs discussed above have been implemented in the public version of the `CPsuperH2.2` code. The output of the two-loop EDM calculations and the strange-quark chromo-EDM is contained in the auxiliary array `RAUX_H`. The additional two-loop EDMs involving charginos and neutralinos have been added to the corresponding EDMs presented in ref. [32] to yield the total EDMs. Specifically, the following assignment of variables (all in units of cm) has been made in the updated code `CPsuperH2.2`:

- Two-loop electron EDMs induced by the γ-$H^{\pm}$-$W^{\mp}$ and γ-$W^{\pm}$-$W^{\mp}$ couplings:

$$\texttt{RAUX\_H(205)} = (d_e^E/e)^{WH^\mp}\,, \quad \texttt{RAUX\_H(206)} = (d_e^E/e)^{WW}\,. \quad \text{(A.12)}$$

- Two-loop down-quark EDMs induced by the γ-$H^{\pm}$-$W^{\mp}$ and γ-$W^{\pm}$-$W^{\mp}$ couplings:

$$\texttt{RAUX\_H(225)} = (d_d^E/e)^{WH^\mp}\,, \quad \texttt{RAUX\_H(226)} = (d_d^E/e)^{WW}\,. \quad \text{(A.13)}$$

- The corresponding two-loop strange-quark EDMs:

$$\texttt{RAUX\_H(235)} = (d_s^E/e)^{WH^\mp}\,, \quad \texttt{RAUX\_H(236)} = (d_s^E/e)^{WW}\,. \quad \text{(A.14)}$$

- The chromo-EDM of the s-quark:

$$\texttt{RAUX\_H(400)} = d_s^C = (d_s^C)^{\tilde{\chi}^\pm} + (d_s^C)^{\tilde{\chi}^0} + (d_s^C)^{\tilde{g}} + (d_s^C)^H\,, \quad \text{(A.15)}$$

  where the individual contributions are given by

$$\begin{aligned} \texttt{RAUX\_H(401)} &= (d_s^C)^{\tilde{\chi}^\pm}\,, \quad \texttt{RAUX\_H(402)} = (d_s^C)^{\tilde{\chi}^0}\,, \\ \texttt{RAUX\_H(403)} &= (d_s^C)^{\tilde{g}}\,, \quad \texttt{RAUX\_H(404)} = (d_s^C)^H\,. \end{aligned} \quad \text{(A.16)}$$

JHEP10(2010)049

References

[1] B.C. Regan, E.D. Commins, C.J. Schmidt and D. DeMille, *New limit on the electron electric dipole moment*, *Phys. Rev. Lett.* **88** (2002) 071805 [SPIRES].

[2] C.A. Baker et al., *An improved experimental limit on the electric dipole moment of the neutron*, *Phys. Rev. Lett.* **97** (2006) 131801 [hep-ex/0602020] [SPIRES].

[3] M.V. Romalis, W.C. Griffith and E.N. Fortson, *A new limit on the permanent electric dipole moment of Hg- 199*, *Phys. Rev. Lett.* **86** (2001) 2505 [hep-ex/0012001] [SPIRES].

[4] W.C. Griffith et al., *Improved Limit on the Permanent Electric Dipole Moment of Hg-199*, *Phys. Rev. Lett.* **102** (2009) 101601 [SPIRES].

[5] H.P. Nilles, *Supersymmetry, Supergravity and Particle Physics*, *Phys. Rept.* **110** (1984) 1 [SPIRES].

[6] H.E. Haber and G.L. Kane, *The Search for Supersymmetry: Probing Physics Beyond the Standard Model*, *Phys. Rept.* **117** (1985) 75 [SPIRES].

[7] For the current status of the CKM model, see: http://ckmfitter.in2p3.fr/, http://www.utfit.org/.

[8] M.S. Carena, J.M. Moreno, M. Quirós, M. Seco and C.E.M. Wagner, *Supersymmetric CP-violating currents and electroweak baryogenesis*, *Nucl. Phys.* **B 599** (2001) 158 [hep-ph/0011055] [SPIRES].

[9] M.S. Carena, M. Quirós, M. Seco and C.E.M. Wagner, *Improved results in supersymmetric electroweak baryogenesis*, *Nucl. Phys.* **B 650** (2003) 24 [hep-ph/0208043] [SPIRES].

[10] T. Konstandin, T. Prokopec, M.G. Schmidt and M. Seco, *MSSM electroweak baryogenesis and flavour mixing in transport equations*, *Nucl. Phys.* **B 738** (2006) 1 [hep-ph/0505103] [SPIRES].

[11] D.J.H. Chung, B. Garbrecht, M.J. Ramsey-Musolf and S. Tulin, *Yukawa Interactions and Supersymmetric Electroweak Baryogenesis*, *Phys. Rev. Lett.* **102** (2009) 061301 [arXiv:0808.1144] [SPIRES].

[12] The LHCb collaboration, et al., *Roadmap for selected key measurements of LHCb*, arXiv:0912.4179 [SPIRES].

[13] EDM collaboration, Y.K. Semertzidis et al., *A new method for a sensitive deuteron EDM experiment*, *AIP Conf. Proc.* **698** (2004) 200 [hep-ex/0308063] [SPIRES].

[14] Y.F. Orlov, W.M. Morse and Y.K. Semertzidis, *Resonance method of electric-dipole-moment measurements in storage rings*, *Phys. Rev. Lett.* **96** (2006) 214802 [hep-ex/0605022] [SPIRES].

[15] O. Lebedev, K.A. Olive, M. Pospelov and A. Ritz, *Probing CP-violation with the deuteron electric dipole moment*, *Phys. Rev.* **D 70** (2004) 016003 [hep-ph/0402023] [SPIRES].

[16] J.R. Ellis, J.S. Lee and A. Pilaftsis, *B-Meson Observables in the Maximally CP-Violating MSSM with Minimal Flavour Violation*, *Phys. Rev.* **D 76** (2007) 115011 [arXiv:0708.2079] [SPIRES].

[17] J. Ellis, R.N. Hodgkinson, J.S. Lee and A. Pilaftsis, *Flavour Geometry and Effective Yukawa Couplings in the MSSM*, *JHEP* **02** (2010) 016 [arXiv:0911.3611] [SPIRES].

JHEP10(2010)049

[18] M. Argyrou, A.B. Lahanas and V.C. Spanos, *Refining the predictions of supersymmetric CP-violating models: A top-down approach*, *JHEP* **05** (2008) 026 [arXiv:0804.2613] [SPIRES].

[19] G. Colangelo, E. Nikolidakis and C. Smith, *Supersymmetric models with minimal flavour violation and their running*, *Eur. Phys. J.* **C 59** (2009) 75 [arXiv:0807.0801] [SPIRES].

[20] W. Altmannshofer, A.J. Buras and P. Paradisi, *Low Energy Probes of CP-violation in a Flavor Blind MSSM*, *Phys. Lett.* **B 669** (2008) 239 [arXiv:0808.0707] [SPIRES].

[21] L. Mercolli and C. Smith, *EDM constraints on flavored CP-violating phases*, *Nucl. Phys.* **B 817** (2009) 1 [arXiv:0902.1949] [SPIRES].

[22] A.L. Kagan, G. Perez, T. Volansky and J. Zupan, *General Minimal Flavor Violation*, *Phys. Rev.* **D 80** (2009) 076002 [arXiv:0903.1794] [SPIRES].

[23] R. Zwicky and T. Fischbacher, *On discrete Minimal Flavour Violation*, *Phys. Rev.* **D 80** (2009) 076009 [arXiv:0908.4182] [SPIRES].

[24] S.M. Carroll, *Lecture notes on general relativity*, gr-qc/9712019 [SPIRES].

[25] T. Ibrahim and P. Nath, *The neutron and the lepton EDMs in MSSM, large CP-violating phases and the cancellation mechanism*, *Phys. Rev.* **D 58** (1998) 111301 [*Erratum ibid.* **D 60** (1999) 099902] [hep-ph/9807501] [SPIRES].

[26] M. Brhlik, L.L. Everett, G.L. Kane and J.D. Lykken, *A resolution to the supersymmetric CP problem with large soft phases via D-branes*, *Phys. Rev. Lett.* **83** (1999) 2124 [hep-ph/9905215] [SPIRES].

[27] T. Falk and K.A. Olive, *Electric Dipole Moment Constraints on Phases in the Constrained MSSM*, *Phys. Lett.* **B 375** (1996) 196 [hep-ph/9602299] [SPIRES].

[28] M. Brhlik, G.J. Good and G.L. Kane, *Electric dipole moments do not require the CP-violating phases of supersymmetry to be small*, *Phys. Rev.* **D 59** (1999) 115004 [hep-ph/9810457] [SPIRES].

[29] V.D. Barger et al., *CP-violating phases in SUSY, electric dipole moments and linear colliders*, *Phys. Rev.* **D 64** (2001) 056007 [hep-ph/0101106] [SPIRES].

[30] D.A. Demir, O. Lebedev, K.A. Olive, M. Pospelov and A. Ritz, *Electric dipole moments in the MSSM at large* $\tan\beta$, *Nucl. Phys.* **B 680** (2004) 339 [hep-ph/0311314] [SPIRES].

[31] K.A. Olive, M. Pospelov, A. Ritz and Y. Santoso, *CP-odd phase correlations and electric dipole moments*, *Phys. Rev.* **D 72** (2005) 075001 [hep-ph/0506106] [SPIRES].

[32] J.R. Ellis, J.S. Lee and A. Pilaftsis, *Electric Dipole Moments in the MSSM Reloaded*, *JHEP* **10** (2008) 049 [arXiv:0808.1819] [SPIRES].

[33] M. Battaglia et al., *Proposed post-LEP benchmarks for supersymmetry*, *Eur. Phys. J.* **C 22** (2001) 535 [hep-ph/0106204] [SPIRES].

[34] B.C. Allanach et al., *The Snowmass points and slopes: Benchmarks for SUSY searches*, *Eur. Phys. J.* **C 25** (2002) 113 [hep-ph/0202233] [SPIRES].

[35] N. Ghodbane and H.-U. Martyn, *Compilation of SUSY particle spectra from Snowmass 2001 benchmark models*, hep-ph/0201233 [SPIRES].

[36] M. Battaglia et al., *Updated post-WMAP benchmarks for supersymmetry*,

JHEP10(2010)049

Eur. Phys. J. **C 33** (2004) 273 [hep-ph/0306219] [SPIRES].

[37] Y. Li, S. Profumo and M. Ramsey-Musolf, *Higgs-Higgsino-Gaugino Induced Two Loop Electric Dipole Moments*, *Phys. Rev.* **D 78** (2008) 075009 [arXiv:0806.2693] [SPIRES].

[38] Y. Li, S. Profumo and M. Ramsey-Musolf, *A Comprehensive Analysis of Electric Dipole Moment Constraints on CP-violating Phases in the MSSM*, *JHEP* **08** (2010) 062 [arXiv:1006.1440] [SPIRES].

[39] Y.K. Semertzidis et al., *Sensitive search for a permanent muon electric dipole moment*, hep-ph/0012087 [SPIRES].

[40] T. Aushev et al., *Physics at Super B Factory*, arXiv:1002.5012 [SPIRES].

[41] M. Pospelov and A. Ritz, *Neutron EDM from electric and chromoelectric dipole moments of quarks*, *Phys. Rev.* **D 63** (2001) 073015 [hep-ph/0010037] [SPIRES].

[42] M. Pospelov and A. Ritz, *Electric dipole moments as probes of new physics*, *Annals Phys.* **318** (2005) 119 [hep-ph/0504231] [SPIRES].

[43] M. Pospelov and A. Ritz, private communications.

[44] CAST collaboration, K. Zioutas et al., *First results from the CERN Axion Solar Telescope (CAST)*, *Phys. Rev. Lett.* **94** (2005) 121301 [hep-ex/0411033] [SPIRES].

[45] CAST collaboration, S. Andriamonje et al., *An improved limit on the axion-photon coupling from the CAST experiment*, *JCAP* **04** (2007) 010 [hep-ex/0702006] [SPIRES].

[46] J.S. Lee et al., *CPsuperH: A computational tool for Higgs phenomenology in the minimal supersymmetric standard model with explicit CP-violation*, *Comput. Phys. Commun.* **156** (2004) 283 [hep-ph/0307377] [SPIRES].

[47] J.S. Lee, M. Carena, J. Ellis, A. Pilaftsis and C.E.M. Wagner, *CPsuperH2.0: an Improved Computational Tool for Higgs Phenomenology in the MSSM with Explicit CP-violation*, *Comput. Phys. Commun.* **180** (2009) 312 [arXiv:0712.2360] [SPIRES].

[48] A. Pilaftsis, *Higgs-boson two-loop contributions to electric dipole moments in the MSSM*, *Phys. Lett.* **B 471** (1999) 174 [hep-ph/9909485] [SPIRES].

[49] D. Chang, W.-F. Chang and W.-Y. Keung, *Additional two-loop contributions to electric dipole moments in supersymmetric theories*, *Phys. Lett.* **B 478** (2000) 239 [hep-ph/9910465] [SPIRES].

[50] T.H. West, *Fermion electric dipole moments induced by P- and T-odd $WW\gamma$ interactions in the minimal supersymmetric standard model and multi-Higgs-boson model*, *Phys. Rev.* **D 50** (1994) 7025 [SPIRES].

[51] T. Kadoyoshi and N. Oshimo, *Neutron electric dipole moment from supersymmetric anomalous W-boson coupling*, *Phys. Rev.* **D 55** (1997) 1481 [hep-ph/9607301] [SPIRES].

[52] D. Chang, W.-F. Chang and W.-Y. Keung, *Electric dipole moment in the split supersymmetry models*, *Phys. Rev.* **D 71** (2005) 076006 [hep-ph/0503055] [SPIRES].

[53] G.F. Giudice and A. Romanino, *Electric dipole moments in split supersymmetry*, *Phys. Lett.* **B 634** (2006) 307 [hep-ph/0510197] [SPIRES].

JHEP10(2010)049